Assignment of the Side-Chain ^1H and ^{13}C Resonances of Interleukin-1β Using Double- and Triple-Resonance Heteronuclear Three-Dimensional NMR Spectroscopy†

G. Marius Clore,*,‡ Ad Bax,‡ Paul C. Driscoll,‡ Paul T. Wingfield,§ and Angela M. Gronenborn*,‡

Laboratory of Chemical Physics, Building 2, National Institute of Diabetes and Digestive and Kidney Diseases, and Protein Expression Laboratory, Building 6B, National Institutes of Health, Bethesda, Maryland 20892

Received March 15, 1990; Revised Manuscript Received May 22, 1990

ABSTRACT: The assignment of the aliphatic ^1H and ^{13}C resonances of IL-1β, a protein of 153 residues and molecular mass 17.4 kDa, is presented by use of a number of novel three-dimensional (3D) heteronuclear NMR experiments which rely on large heteronuclear one-bond J couplings to transfer magnetization and establish through-bond connectivities. These 3D NMR experiments circumvent problems traditionally associated with the application of conventional 2D ^1H–^1H correlation experiments to proteins of this size, in particular the extensive chemical shift overlap which precludes the interpretation of the spectra and the reduced sensitivity arising from ^1H line widths that are often significantly larger than the ^1H–^1H J couplings. The assignment proceeds in two stages. In the first step the $^{13}C\alpha$ chemical shifts are correlated with the NH and ^{15}N chemical shifts by a 3D triple-resonance NH–^{15}N–$^{13}C\alpha$ (HNCA) correlation experiment which reveals both intraresidue NH(i)–^{15}N(i)–$^{13}C\alpha$(i) and some weaker interresidue NH(i)–^{15}N(i)–Cα(i–1) correlations, the former via intraresidue one-bond $^1J_{NC\alpha}$ and the latter via interresidue two-bond $^2J_{NC\alpha}$ couplings. As the NH, ^{15}N, and C$^\alpha$H chemical shifts had previously been sequentially assigned by 3D ^1H Hartmann–Hahn ^{15}N–^1H multiple quantum coherence (3D HOHAHA-HMQC) and 3D heteronuclear ^1H nuclear Overhauser ^{15}N–^1H multiple quantum coherence (3D NOESY-HMQC) spectroscopy [Driscoll, P. C., Clore, G. M., Marion, D., Wingfield, P. T., & Gronenborn, A. M. (1990) *Biochemistry 29*, 3542–3556], the 3D triple-resonance HNCA correlation experiment permits the sequence-specific assignments of $^{13}C\alpha$ chemical shifts in a straightforward manner. The second step involves the identification of side-chain spin systems by 3D ^1H–^{13}C–^{13}C–^1H correlated (HCCH-COSY) and 3D ^1H–^{13}C–^{13}C–^1H total correlated (HCCH-TOCSY) spectroscopy, the latter making use of isotropic mixing of ^{13}C magnetization to obtain relayed connectivities along the side chains. Extensive cross-checks are provided in the assignment procedure by examination of the connectivities between ^1H resonances at all the corresponding ^{13}C shifts of the directly bonded ^{13}C nuclei. In this manner, we were able to obtain complete ^1H and ^{13}C side-chain assignments for all residues, with the exception of 4 (out of a total of 15) lysine residues for which partial assignments were obtained. The 3D heteronuclear correlation experiments described are highly sensitive, and the required set of three 3D spectra was recorded in only 1 week of measurement time on a single uniformly $^{15}N/^{13}C$-labeled 1.7 mM sample of interleukin-1β. This first example of the essentially complete side-chain assignments of a protein with a molecular mass greater than 15 kDa by heteronuclear 3D NMR methods provides a basis for the determination of a full high-resolution three-dimensional structure of interleukin-1β in solution.

Interleukin-1β (IL-1β)[1] is a member of the cytokine family of proteins, which play a central role in the immune and inflammatory responses. It is a protein of 153 amino acids with a molecular mass of 17.4 kDa, and its wide-ranging biological activities include stimulation of B-lymphocyte proliferation and fever induction [see Oppenheim et al. (1986), Dinarello (1988), and Moore (1989) for reviews]. In two recent papers we presented the complete assignment of the ^{15}N and ^1H resonances of the polypeptide backbone of IL-1β and the determination of its secondary structure and molecular topology using 3D heteronuclear ^1H–^{15}N NMR spectroscopy (Driscoll et al., 1990a,b). At that time only a limited number of ^1H side-chain resonance assignments were obtained owing to two factors. First, the sensitivity of homonuclear J correlation experiments (COSY, P.COSY, DQF-COSY, HOHAHA, etc.) is reduced in larger proteins owing to their slow tumbling, which results in ^1H line widths that are often significantly larger than many of the ^1H–^1H couplings. As a result, only a limited number of relayed through-bond connectivities were observed in the ^1H–^{15}N 3D HOHAHA-HMQC experiments, thereby preventing in the majority of cases the correlation of NH chemical shifts with those of side-chain protons (C$^\beta$H and beyond). Second, extensive chemical shift overlap in the aliphatic region of the 2D ^1H–^1H

† This work was supported by the Intramural AIDS Anti-viral Program of the Office of the Director of the National Institutes of Health (G.M.C., A.M.G., A.B., and P.T.W.).

‡ Laboratory of Chemical Physics.

§ Protein Expression Laboratory.

[1] Abbreviations: IL-1β, interleukin-1β; COSY, correlated spectroscopy; HOHAHA, homonuclear Hartmann–Hahn spectroscopy; TOCSY, total correlated spectroscopy; HMQC, heteronuclear multiple quantum correlation spectroscopy; DQF-COSY, double quantum filtered correlated spectroscopy; P.COSY, primitive correlated spectroscopy; HNCA, 3D triple-resonance NH–^{15}N–$^{13}C\alpha$ correlation spectroscopy; HCCH-COSY, 3D ^1H–^{13}C–^{13}C–^1H correlation spectroscopy via $^1J_{CC}$ carbon couplings; HCCH-TOCSY, 3D ^1H–^{13}C–^{13}C–^1H total correlation spectroscopy with isotropic mixing of ^{13}C magnetization; ^1H–^{13}C NOESY-HMQC, 3D heteronuclear ^1H nuclear Overhauser ^{13}C–^1H multiple quantum coherence spectroscopy; ^1H–^{15}N NOESY-HMQC, 3D heteronuclear ^1H nuclear Overhauser ^{15}N–^1H multiple quantum coherence spectroscopy; ^1H–^{15}N HOHAHA-HMQC, 3D heteronuclear ^1H Hartmann–Hahn ^{15}N–^1H multiple quantum coherence spectroscopy; NOE, nuclear Overhauser effect; rf, radiofrequency.

P.COSY and HOHAHA spectra, coupled once again with only limited relayed transfers in the relayed COSY and HOHAHA spectra, rendered assignments difficult, particularly for the longer side chain amino acids.

To circumvent these problems, we have resorted to techniques that do not rely on the poorly resolved ^1H–^1H J couplings to establish through-bond connectivities but, instead, utilize the well-resolved one-bond ^1H–^{13}C, ^{13}C–^{13}C, ^1H–^{15}N, and ^{15}N–$^{13}C\alpha$ J couplings to transfer magnetization (Kay et al., 1990a,b; Ikura et al., 1990a; Fesik et al., 1990; Bax et al., 1990a,b). In this paper, we demonstrate that a variety of 3D experiments based on these heteronuclear couplings enable assignments of the side-chain ^1H and ^{13}C resonances to be obtained with relative ease. The strategy involved comprises two stages. In the first step the NH and ^{15}N chemical shifts, which had been previously assigned from the 3D ^1H–^{15}N NOESY-HMQC and HOHAHA-HMQC spectra (Driscoll et al., 1990a), are correlated with $^{13}C\alpha$ chemical shifts by use of a triple-resonance 3D correlation experiment. This is followed by the second step in which the identification of side-chain spin systems is achieved by 3D ^1H–^{13}C–^{13}C–^1H (HCCH)-COSY and HCCH-TOCSY spectroscopy. The latter is a hybrid of the HCCH-COSY (Kay et al., 1990a; Bax et al., 1990a) and CCH-TOCSY (Fesik et al., 1990) experiments and utilizes isotropic mixing of ^{13}C magnetization to obtain relayed connectivities along the side chain. By this mean, we were able to obtain, with the exception of only 4 (out of a total of 15) lysines, complete ^1H and ^{13}C assignments for the side-chain resonances of IL-1β. These assignments lay the groundwork for interpreting the 3D ^1H–^{15}N and ^1H–^{13}C NOESY-HMQC spectra, as well as the 4D $^{13}C/^{15}N$ and $^{13}C/^{13}C$ edited NOESY spectra (Kay et al., 1990c), to obtain a large number of approximate interproton distance restraints required for a full high-resolution three-dimensional structure determination of IL-1β in solution. In addition, the ^{13}C assignments provide a large database of ^{13}C chemical shifts in proteins, supplementing the data previously available on isolated amino acids and small peptides.

Experimental Procedures

IL-1β Preparation and ^{13}C and ^{15}N Labeling. Recombinant Il-1β was prepared with *Escherichia coli* harboring the expression vector derived from pPLc24 (Buell et al., 1985) in which Il-1β is expressed under the control of bacteriophage λP_L promoter and the ribosome binding site of the bacteriophage Mu *ner* gene (Wingfield et al., 1986). Uniform ^{15}N and ^{13}C labeling to a level of >95% was obtained by growing the bacteria in minimal medium with $^{15}NH_4Cl$ and [$^{13}C_6$]-glucose (Isotec Inc. and MSD Isotopes) as the sole nitrogen and carbon sources, respectively. IL-1β was purified as described previously (Wingfield et al., 1986; Gronenborn et al., 1986). The sample for the NMR experiments contained 1.7 mM uniformly $^{15}N/^{13}C$-labeled IL-1β in 90 mM sodium phosphate buffer, pH 5.4, dissolved in either 99.996% D_2O (for the 3D HCCH-COSY, HCCH-TOCSY, and ^{13}C–^1H NOESY-HMQC experiments) or 90% H_2O/10% D_2O (for the 3D HNCA experiment).

NMR Spectroscopy. All NMR experiments were carried out at 36 °C on either a Bruker AM600 or a Bruker AM500 spectrometer, operating in the "reverse" mode. The pulse sequences used for the 3D triple-resonance HN–^{15}N–$^{13}C\alpha$ correlation experiment (HNCA; Ikura et al., 1990a; Kay et al., 1990b) and the 3D double-resonance HCCH-COSY (Kay et al., 1990a; Bax et al., 1990a) and HCCH-TOCSY (Bax et al., 1990b) experiments have been described in detail previously and therefore will only be summarized below.

The pulse sequence for the 3D HNCA experiment is

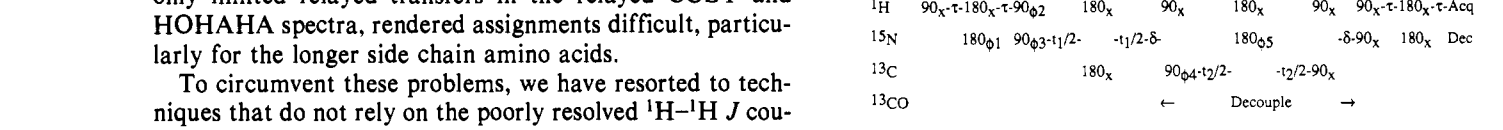

The phase cycling used is as follows: $\phi1 = x,-x$; $\phi2 = y,-y$; $\phi3 = x$; $\phi4 = 2(x),2(-x)$; $\phi5 = 4(x),4(y),4(-x),4(-y)$; Acq = $x,-x,-x,x,-x,x,x,-x$. The phases $\phi3$ and $\phi4$ are independently incremented by 90° to generate complex data in the t_1 and t_2 dimensions, respectively, and quadrature detection in both the t_1 and t_2 dimensions is achieved according to the TPPI-States method (Marion et al., 1989). The delay δ (33 ms) is adjusted to an integral value of $1/J_{NH}$ to ensure that ^{15}N magnetization remains antiphase with respect to the coupled proton and to approximately $1/(3J_{NC\alpha})$ to minimize relaxation losses and optimize transfer between the ^{15}N and $^{13}C\alpha$ spins where significant ^{15}N–$^{13}C\alpha$ coupling is present. The delay τ is set to 2.25 ms, slightly shorter than $1/(4J_{NH})$ to minimize relaxation losses. The HNCA experiment was recorded on a 500-MHz spectrometer equipped with a 5-mm triple-resonance probe head with the inner coil tuned to ^1H and ^2H and the outer coil tuned to ^{13}C and ^{15}N. The ^{15}N pulses were generated by the X channel of the spectrometer, while the $^{13}C\alpha$ and ^{13}CO pulses were generated with two additional frequency synthesizers. ^{13}CO and ^{15}N decoupling were achieved with GARP (Shaka et al., 1985) and WALTZ (Shaka et al., 1983) modulation, respectively. The ^1H carrier was placed at 8.67 ppm, the ^{15}N carrier at 118.5 ppm, and the $^{13}C\alpha$ carrier at 56 ppm. Suppression of the water resonance was carried out with off-resonance DANTE-style presaturation of the H_2O signal (Kay et al., 1989). A total of 32 complex t_1 (^{15}N), 64 complex t_2 (^{13}C), and 512 real t_3 (^1H) data points were collected with acquisition times of 30.08 (t_1), 14.85 (t_2), and 64 ms (t_3) and spectral widths of 1064.28 Hz (t_1), 4310 Hz (t_2), and 4000 Hz (t_3). The total measurement time for this experiment was approximately 32 h.

The pulse sequence for the 3D HCCH-COSY experiment is

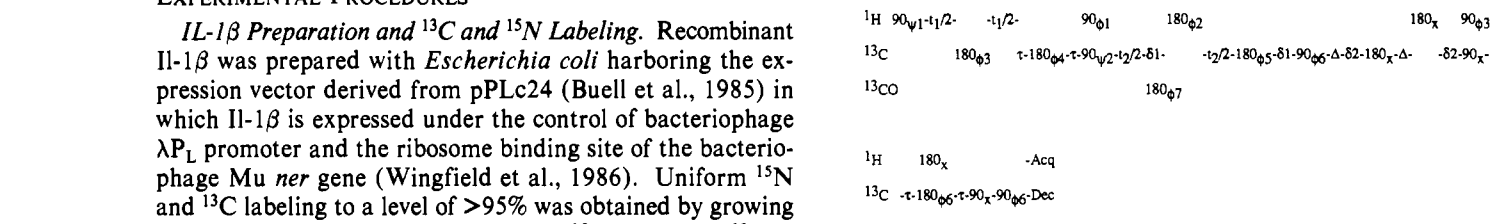

and that for the HCCH-TOCSY experiment is

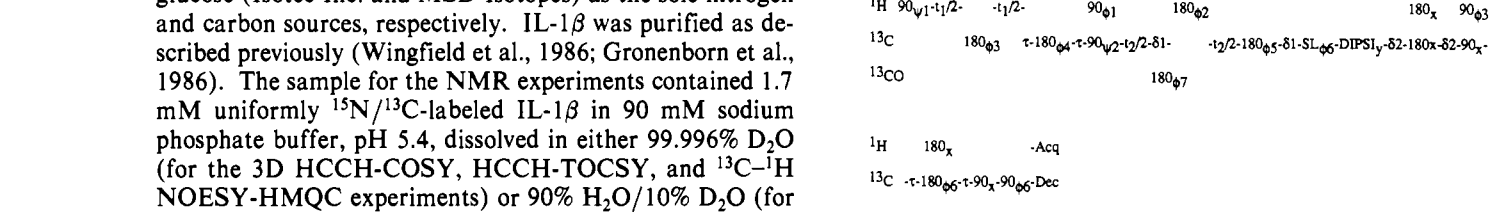

The phase cycling for both experiment is as follows: $\phi1 = y,-y$; $\phi2 = 4(x),4(y),4(-x),4(-y)$; $\phi3 = 8(x),8(-x)$; $\phi4 = 2(x),2(-x)$; $\phi5 = 2(x),2(y),2(-x),2(-y)$; $\phi6 = 4(x),4(-x)$; $\phi7 = 8(x),8(y)$; Acq = $2(x,-x,-x,x),2(-x,x,x,-x)$. Quadrature detection in the t_1 and t_2 dimensions is obtained with the TPPI-States method (Marion et al., 1989) using $\psi1 = 16(x),16(y)$ and $\psi2 = 32(x),32(y)$. Each time t_1 is incremented, the receiver reference phase and $\psi1$ are incremented by 180°; similarly, each time t_2 is incremented, the receiver phase and $\psi2$ are incremented by 180°. Data obtained for $\psi1 = x,y$ and $\psi2 =$

x,y are stored separately and processed as complex data. The $180_{\phi 3}$ and $180_{\phi 4}$ pulses are composite 180° pulses (of the $90_x180_y90_x$ variety). The ^1H and ^{13}C carriers were positioned at 3 and 43 ppm, respectively. The carbonyl $180_{\phi 7}$ pulse used to decouple the carbonyls is applied as a DANTE series (Kay et al., 1989) consisting of eight cycles of six 4°–5° pulses, with the phase of each successive pulse decremented by 60°. The duration of each cycle is set to $1/\delta$ ($\sim$50–60 μs), where δ is the offset of the carbonyl resonances from the ^{13}C rf carrier. In the case of the HCCH-TOCSY experiment, the duration of the spin-lock trim pulse (SL) is 2 ms, and all the pulses of the DIPSI-3 isotropic mixing sequence (Shaka et al., 1988) are applied along the $\pm y$ axis with a 7-kHz rf field strength. The length used for the DIPSI-3 isotropic mixing period was 24 ms. The delay τ is set to 1.5 ms, slightly less than $1/(4J_{CH})$; the delays $\delta 1$ and $\delta 2$ are set to $\sim 1/(6J_{CH}) \sim 1.1$ ms, and the delay $\Delta+\delta 1$ is set to $\sim 1/(8J_{CC}) \sim 3.25$ ms. To eliminate the need for phase correction in the F_1 dimension, the duration of the composite 180° ^{13}C pulse (100 μs) was added to the τ delay between the 180_x and $90_{\phi 1}$ ^1H pulses. In the F_2 dimension, phase correction is eliminated by applying the $180_{\phi 2}$ ^1H pulse at the end of the first $\delta 1$ interval. ^{13}C decoupling during the acquisition period (t_3) is achieved with GARP (Shaka et al., 1985) modulation. The HCCH-COSY experiment was recorded at 600 MHz while the HCCH-TOCSY one was recorded at 500 MHz. A total of 128 complex t_1 (^1H), 32 complex t_2 (^{13}C), and 512 real t_3 (^1H) data points were collected for both experiments with acquisition times of 28.16 (t_1), 10.24 (t_2) and 47.62 (t_3) ms for the HCCH-COSY experiment at 600 MHz and acquisition times of 33.79 (t_1), 12.29 (t_2), and 51.2 (t_3) ms for the HCCH-TOCSY experiment at 500 MHz. Thus, the spectral widths in the F_1 and F_2 dimensions were the same for both experiments, 7.57 and 20.71 ppm, respectively, while the F_3 spectral width was 8.96 ppm for the HCCH-COSY experiment and 10 ppm for the HCCH-TOCSY experiment. The total measurement time for each experiment was approximately 70 h. Because the F_2 spectral width for both experiments was set to 20.71 ppm, extensive folding occurs in this dimension, and each ^{13}C slice contains resonances corresponding to three different ^{13}C chemical shifts.

In addition to the three correlation experiments, we also recorded a ^1H–^{13}C NOESY-HMQC experiment (Ikura et al., 1990b; Zuiderweg et al., 1990) at 600 MHz with a 130-ms (τ_m) NOESY mixing time using the pulse sequence

^1H $90_{\phi 1}$- t_1 -90_x-τ_m-90_x- $180_{\phi 2}$ Acq

^{13}C Dec Δ-90_ψ-$t_2/2$- -$t_2/2$-90_x-Δ-Dec

with phases $\phi 2 = 4(x),4(y)$ and Acq $= x,2(-x),x,-x,2(x),-x$. Quadrature in F_1 and F_2 is obtained with the TPPI-States method (Marion et al., 1989), with $\phi 1 = 4(x,-x),4(y,-y)$ and $\psi = 4[2(x),2(-x)],4[2(y),2(-y)]$ and data for $\phi 1 = x,y$ and $\psi = x,y$ being stored separately to be processed as complex data. Each time t_1 is incremented, $\phi 1$ and the receiver phase are incremented by 180°; and similarly, each time t_2 is incremented, ψ and the receiver phase are incremented by 180°. ^{13}C decoupling during the t_1 and acquisition periods is achieved with GARP (Shaka et al., 1985) modulation. The delay Δ is set to 3 ms, slightly less than $1/(2J_{CH})$. For convenience the initial t_2 delay is adjusted such that the phase correction in F_2 is −180° for the first-order phase and 90° for the zero-order phase by setting $\Delta t_2/2 = [\tau_{180}(^1H) + 4\tau_{90}(^{13}C)/\pi + t_2(0)]$ by appropriate adjustment of $t_2(0)$ (where Δt_2 is the increment used in the t_2 dimension). The ^1H carrier was placed at 3.5 ppm and the ^{13}C carrier at 71.8 ppm. A total of 128 complex t_1 (^1H), 64 complex t_2 (^{13}C), and 512 real t_3 (^1H) data points were collected with acquisition times of 24.32 (t_1), 10.24 (t_2), and 47.62 (t_3) ms, corresponding to sweep widths of 8.76 (F_1), 41.42 (F_2), and 10.41 (F_3) ppm. Thus, the sweep width employed in the ^{13}C F_2 dimension was exactly double that used for the HCCH-COSY and HCCH-TOCSY experiments. By this means, any possible ambiguities in ^{13}C chemical shifts arising from folding are easily resolved by comparing the two sets of experiments. In addition, the NOESY-HMQC spectrum provides an easy means of assigning the ^{13}C chemical shifts of aromatic carbons bound to protons.

Processing of 3D Spectra. All 3D NMR experiments were processed on a Sun Sparc workstation using a simple in-house-written routine for the F_2 Fourier transform together with the commercially available software package NMR2 (New Methods Research, Inc., Syracuse, NY) for processing the F_1–F_3 planes, as described previously (Kay et al., 1989). Zero-filling (once in each dimension) was employed to yield a final absorptive spectrum of 128 × 64 × 512 data points for the HNCA spectrum, 256 × 64 × 512 data points for the HCCH-COSY and HCCH-TOCSY spectra, and 256 × 128 × 512 data points for the NOESY-HMQC spectrum. The weighting function applied in the F_1 and F_3 dimensions was a singly 60°-shifted sine bell window function, while a doubly shifted sine bell function, shifted by 60° at the beginning of the window and 10° at the end of the window, was used in the F_2 dimension (Kay et al., 1989; Driscoll et al., 1990a).

Results and Discussion

The NH, $C^\alpha H$, and ^{15}N chemical shifts had previously been assigned unambiguously by the 3D ^1H–^{15}N HOHAHA-HMQC and NOESY-HMQC experiments (Driscoll et al., 1990a). Because of extensive overlap of $C^\alpha H$ chemical shifts, a helpful first step in the assignment of side chains involves the sequence-specific identification of $^{13}C\alpha$ chemical shifts. For larger proteins with many degenerate $C^\alpha H$ chemical shifts, the $^{13}C\alpha$ shifts cannot simply be determined by recording a 2D ^1H–^{13}C shift correlation spectrum (Brühweiler & Wagner, 1986), and a more sophisticated approach is required. To correlate the $C^\alpha H$ and $^{13}C\alpha$ chemical shifts of a given residue unambiguously, we proceeded to use the 3D NH–^{15}N–$^{13}C\alpha$ (HNCA) triple-resonance correlation experiment, which links the intraresidue NH, ^{15}N, and $^{13}C\alpha$ chemical shifts via the large (95 Hz) one-bond $^1J_{NH}$ coupling and the relatively small (8–12 Hz) one-bond $^1J_{NC\alpha}$ intraresidue coupling (Ikura et al., 1990a; Kay et al., 1990b). Briefly, the HNCA experiment transfers magnetization originating on an NH proton to its directly bonded ^{15}N spin via an INEPT sequence, followed by the evolution of ^{15}N chemical shifts during the period t_1. Subsequent application of 90° pulses to both ^1H and $^{13}C\alpha$ spins establishes three-spin NH–^{15}N–$^{13}C\alpha$ coherence, and the evolution of solely $^{13}C\alpha$ chemical shifts during the period t_2 is ensured by refocusing of ^1H and ^{15}N chemical shifts through the application of ^1H and ^{15}N 180° pulses at the midpoint of the t_2 period. Magnetization is then transferred back to the NH protons by simply reversing the above procedure. The end result is a 3D spectrum in which each peak is labeled by ^{15}N, $^{13}C\alpha$, and NH chemical shifts in the F_1, F_2, and F_3 dimensions, respectively.

Several slices of the 3D HNCA spectrum at different ^{15}N-(F_1) chemical shifts are shown in Figure 1. It will be noted that, in addition to the intraresidue NH(i)–^{15}N(i)–Cα(i) correlations, there are also weaker interresidue NH(i)–^{15}N-(i)–Cα(i−1) correlations which arise via the small ($\leq$7 Hz) two-bond $^2J_{NC\alpha}$ interresidue coupling. A total of 61 such sequential connectivities were observed, all of which confirmed the previous assignments. Further, these interresidue two-bond J connectivities enabled us to obtain the $^{13}C\alpha$ chemical shift

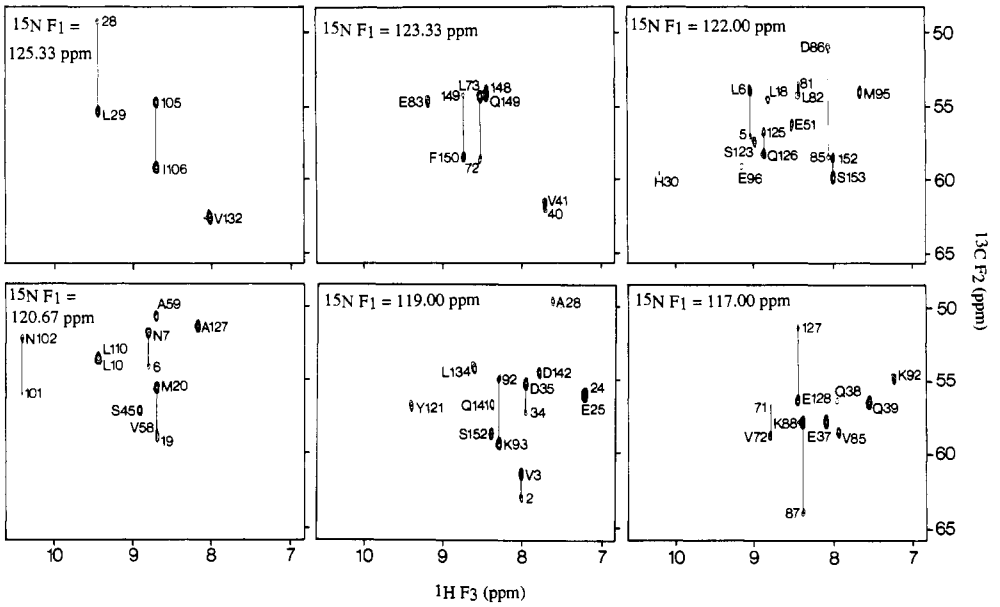

FIGURE 1: Representative slices at six different $^{15}N(F_1)$ chemical shifts of the 3D HNCA spectrum of uniformly $^{15}N/^{13}C$-labeled IL-1β. The intraresidue NH(i)–$^{15}N(i)$–$^{13}C\alpha(i)$ correlations are indicated by the residue name and number, while the weaker interresidue NH(i)–$^{15}N(i)$–$^{13}C\alpha(i-1)$ cross-peaks are indicated by residue number only.

assignments for seven of the eight proline residues [see for example the Val-3(NH)–Val-3(^{15}N)–Pro-2($^{13}C\alpha$) cross-peak at $\delta^{15}N$ = 119 ppm in Figure 1]. From the HNCA experiment alone we were able to obtain the $^{13}C\alpha$ chemical shifts for all but nine residues (Ala-1, Ser-17, Asn-53, Leu-62, Lys-63, Pro-91, Ser-114, Ile-143, and Thr-144) which did not show any correlations peaks. This may be due to either significant line broadening of the NH, ^{15}N, or $^{13}C\alpha$ line widths or to a reduction in NH resonance intensity arising from NOE effects. The latter is due to the selective presaturation employed to suppress the water signal and may involve either bound water or C$^\alpha$H protons degerate with the water resonance or rapidly exchanging side-chain amide and guanidinium groups. In the case of Leu-62 and Lys-63, the absence of HNCA correlation peaks is in all likelihood due to the large ^{15}N line widths for these two residues arising from exchange contributions to T_2 (Clore et al., 1990b).

With all the C$^\alpha$H resonance assignments in hand, together with the large majority of $^{13}C\alpha$ assignments obtained from the HNCA experiment, it is now possible to use the HCCH-COSY (Bax et al., 1990a) and HCCH-TOCSY (Bax et al., 1990b) experiments to delineate the amino acid spin systems. The basis of the two experiments is similar, and they make use of the well-resolved one-bond ^1H–^{13}C (~140 Hz) and ^{13}C–^{13}C (30–40 Hz) J couplings to transfer magnetization, thereby circumventing the problems associated with conventional methodologies (e.g., ^1H–^1H COSY, HOHAHA, etc.) which rely on the poorly resolved (<12 Hz) ^1H–^1H J couplings. The scheme for the two experiments is also similar. In the first step, ^1H magnetization from a proton is transferred to its directly bonded ^{13}C nucleus via the $^1J_{CH}$ coupling in an INEPT-type manner. In the second step, ^{13}C magnetization is transferred to its ^{13}C neighbor(s) via the $^1J_{CC}$ coupling. In the case of the HCCH-COSY experiment, this is achieved by a 90° ^{13}C COSY mixing pulse so that magnetization is only transferred from a ^{13}C nucleus to its directly bonded ^{13}C neighbors; in the HCCH-TOCSY experiment, on the other hand, isotropic mixing of ^{13}C spins is achieved such that both direct and multiple relayed magnetization transfer occurs along the carbon chain (Fesik et al., 1990; Bax et al., 1990b). Finally, ^{13}C magnetization is transferred back to ^1H via the $^1J_{CH}$ coupling. The final result is a 3D spectrum in which each $^1H(F_1)$–$^1H(F_3)$ plane has an appearance similar to that of a 2D ^1H–^1H COSY or HOHAHA/TOCSY experiment but is edited by the ^{13}C chemical shift of the ^{13}C nucleus directly bonded to the ^1H at the diagonal position from which magnetization originates. Further, in contrast to the 2D correlation experiments, the cross-peaks in each plane do not occur symmetrically on either side of the diagonal. This is represented diagrammatically in Figure 2. Consider the case where magnetization is transferred from proton A to proton B. In the plane corresponding to the ^{13}C chemical shift of the ^{13}C nucleus directly bonded to proton A where magnetization originates, a correlation is observed between a diagonal peak at $(F_1,F_3) = (\delta_A,\delta_A)$ and a cross-peak at $(F_1,F_3) = (\delta_A,\delta_B)$ in half of the spectrum. The symmetric correlation between the diagonal peak at $(F_1,F_3) = (\delta_B,\delta_B)$ and the cross-peak at $(F_1,F_3) = (\delta_B,\delta_A)$ is then seen in the plane corresponding to the ^{13}C chemical shift of the ^{13}C nucleus directly bonded to proton B. By this means, unambiguous checks on the assignments are afforded at each step in the process, which are made all the easier as the ^{13}C chemical shifts for different carbon types are located in characteristic regions of the ^{13}C spectrum with

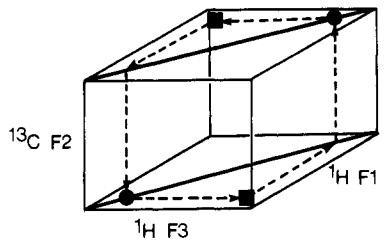

FIGURE 2: Schematic diagram of two slices of an HCCH spectrum at different $^{13}C(F_2)$ chemical shifts showing the diagonal and cross-peaks expected for a simple two-spin system. The diagonal peaks are represented by circles and the cross-peaks by squares. Note that each slice is asymmetric about the diagonal, and cross-peaks only appear in the F_3 dimension. This is due to the fact that magnetization originating from a proton attached to a given ^{13}C nucleus is only visible in the F_2 slice corresponding to the ^{13}C chemical shift of this particular ^{13}C nucleus. The corresponding cross-peak at the other side of the $F_1 = F_3$ diagonal is found in the slice taken at the ^{13}C frequency of the destination carbon.

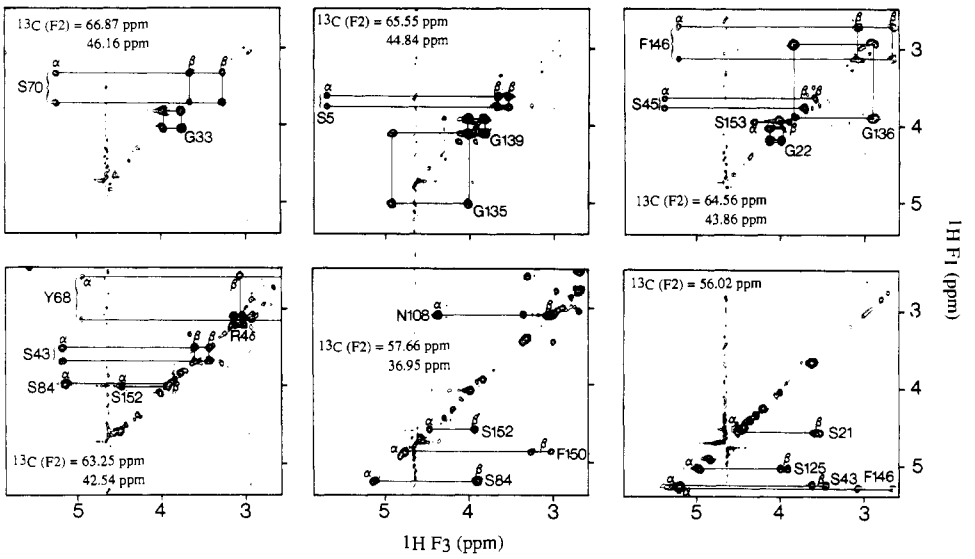

FIGURE 3: Selected slices at different $^{13}C(F_2)$ chemical shifts of the HCCH-COSY spectrum of uniformly $^{15}N/^{13}C$-labeled IL-1β, principally illustrating connectivities involving Gly and Ser residues. Note, that owing to the small sweep width (20.71 ppm) employed in the $^{13}C(F_2)$ dimension, extensive folding occurs, so that each slice corresponds to several ^{13}C chemical shifts with a separation of 20.71 ppm. Note that the separation between successive slices in the F_2 dimension is 0.32 ppm (48 Hz), so that cross-peaks originating from a particular proton may appear in adjacent slices.

little overlap between them (Howarth & Lilley, 1978). This feature also permits one to use extensive folding in the $^{13}C(F_2)$ dimension without the risk of introducing ambiguities. Further, this enables one to resolve problems associated with extensive chemical shift degeneracy. For example, even if the $C^{\alpha}H$, $^{13}C\alpha$, and $C^{\beta}H$ chemical shifts of two residues are degenerate, one can still ascertain that two residues rather than one are involved and trace out the connectivities for the remainder of the two spin systems, providing the $^{13}C\beta$ chemical shifts of the two residues are different.

The HCCH-COSY experiment is particularly useful for identifying Gly, Ala, Thr, and Val spin systems, as well as amino acids of the AMX type (e.g., Ser, Cys, Asn, Asp, His, Tyr, Phe, and Trp). This is illustrated in Figures 3–5. Figure 3 principally demonstrates the use of the HCCH-COSY experiment for the assignment of Gly and Ser spin systems. Both these residues tend to pose problems in conventional ^1H–^1H correlation spectra as the proton resonances are often very close to each other. Each slice corresponds to several ^{13}C shifts separated by 20.71 ppm. Gly $^{13}C\alpha$ shifts occur at 42–46 ppm, while $^{13}C\alpha$ and $^{13}C\beta$ shifts of Ser occur at 55–60 and 61–67 ppm, respectively. The two Gly $C^{\alpha}H$ protons are attached to the same $C\alpha$ carbon, so that a symmetric pattern appears about the diagonal. The same is true, of course, for β-methylene protons. However, the β-methylene protons are also associated with cross-peaks to the $C^{\alpha}H$ proton. Consequently, there is no difficulty in deciding which peaks originate from $C^{\alpha}H$ protons of Gly and $C^{\beta}H$ protons of either Ser (left-hand and middle top panels of Figure 3) or another AMX spin system such as Phe whose $C\beta$ has a chemical shift similar to that of the Gly $C\alpha$ (right-hand top panel of Figure 3). The assignment of the Ser spin system is easily checked by examining the slices corresponding to the $C\alpha$ and $C\beta$ chemical shifts of Ser (e.g., left-hand and middle bottom panels of Figure 3). In this respect, we note that in conventional ^1H–^1H correlated spectra it is often difficult to ascertain the $C^{\alpha}H$ and $C^{\beta}H$ chemical shifts of Ser for cases where the $C^{\beta}H$ shifts are degenerate, as the latter may lie to both low and high field of the $C^{\alpha}H$ shifts. In the case of the HCCH-COSY experiment, this is simply resolved as the ^{13}C chemical shifts of the $C\alpha$ and $C\beta$ carbons differ by 2–10 ppm, with the $C\alpha$ resonance

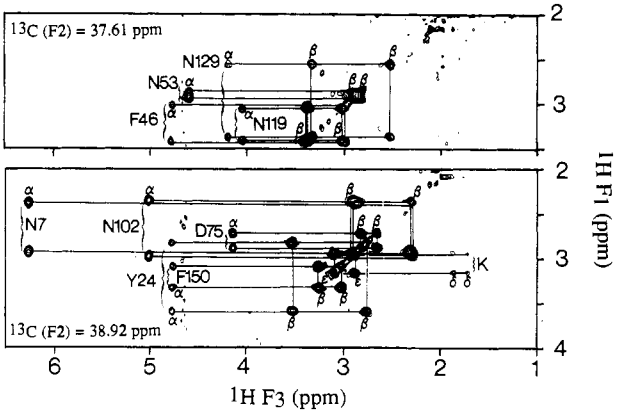

FIGURE 4: Selected slices at different ^{13}C (F_2) chemical shifts of the HCCH-COSY spectrum of uniformly $^{15}N/^{13}C$-labeled IL-1β illustrating connectivities from the $C^{\beta}H$ to $C^{\alpha}H$ protons for AMX spin systems. In the bottom panel, two cross-peaks from the $C^{\epsilon}H$ to the $C^{\delta}H$ protons of a lysine residue are assigned. These peaks originate from one of the four lysine residues (out of a total of 15 lysines present in IL-1β) for which complete side-chain assignments could not be obtained.

always upfield of the $C\beta$ one. Examples of other cross-peaks arising from the $C^{\beta}H$ protons of AMX spin systems are illustrated in Figure 4 for a number of Tyr, Phe, Asn, and Asp residues. The assignment of Ala spin systems is also completely straightforward as only two ^{13}C and ^1H shifts are involved.

Thr and Val spin systems display characteristic connectivities originating from the $C^{\beta}H$ protons to the $C^{\alpha}H$ and $C^{\gamma}H$ methyl protons. The Thr $C\beta$ chemical shifts are at 70–73 ppm, while those of Val are at 31–37 ppm, so the cross-peaks arising from a $C^{\beta}H$ proton of a Val or Thr residue can be distinguished (irrespective of arguments based on $C^{\beta}H$ chemical shifts) even when the chemical shifts of the two methyl proton resonances of Val are degenerate. Some examples of connectivities arising from the $C^{\beta}H$ proton of Thr are illustrated in Figure 6 (middle panel).

Despite the resolution afforded by the $^{13}C(F_2)$ dimension in the HCCH-COSY experiment, problems still remain with regard to the assignment of other spin systems. For example,

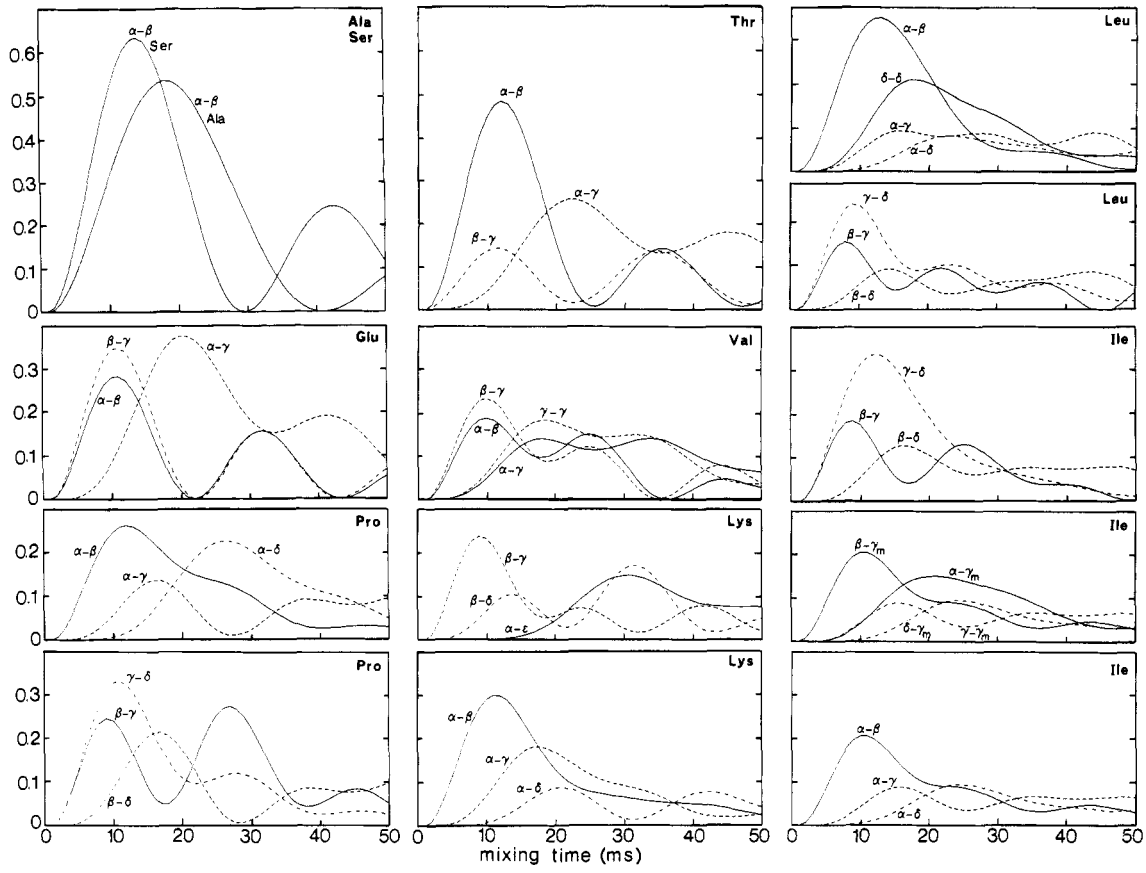

FIGURE 5: Amount of net intraresidue carbon–carbon magnetization transfer occurring during the DIPSI-3 mixing period in the HCCH-TOCSY experiment, assuming a relaxation rate of ^{13}C magnetization during isotropic mixing equal to 33 s^{-1}. Because of J_{CC} dephasing during the $\delta 1$, $\delta 2$, and t_2 periods in the pulse sequence (see Experimental Procedures), the curves should be shifted toward the left by several milliseconds for predicting the cross-peak intensities observed in the HCCH-TOCSY spectrum. Cross-peak intensities in the HCCH-TOCSY experiment are proportional to the amount of carbon–carbon magnetization transfer but are attenuated 2-fold if one of the carbons has two magnetically inequivalent protons attached and 4-fold if both carbons have nonequivalent protons attached. Reduced effective carbon–carbons J couplings (Bax et al., 1990b) have been used for calculating these graphs: Ser, $J_{\alpha\beta}$ = 35 Hz; Ala, $J_{\alpha\beta}$ = 25 Hz; Thr, $J_{\alpha\beta}$ = 20 Hz, $J_{\beta\gamma}$ = 35 Hz; Glu, $J_{\alpha\beta}$ = 30 Hz; $J_{\beta\gamma}$ = 33 Hz; Val, $J_{\alpha\beta}$ = 27 Hz, $J_{\beta\gamma}$ = 30 Hz; Pro, $J_{\alpha\beta}$ = 27 Hz, $J_{\beta\gamma}$ = $J_{\gamma\delta}$ = 33 Hz; Lys, $J_{\alpha\beta}$ = 30 Hz, $J_{\beta\gamma}$ = $J_{\beta\delta}$ = $J_{\delta\epsilon}$ = 33 Hz; Leu, $J_{\alpha\beta}$ = $J_{\beta\gamma}$ = 30 Hz, $J_{\gamma\delta}$ = 33 Hz; Ile, $J_{\alpha\beta}$ = $J_{\beta\gamma m}$ = 27 Hz, $J_{\beta\gamma}$ = $J_{\gamma\delta}$ = 30 Hz. All multiple-bond carbon–carbon couplings are assumed to be zero, and couplings between aliphatic and carbonyl resonances have been neglected because the large resonance chemical shift difference between the aromatic and carbonyl nuclei on the one hand and the aliphatic carbons on the other reduces their effective J couplings to aliphatic carbons (Shaka et al., 1988; Bax et al., 1990b).

it is frequently the case for Gln, Glu, Met, and Leu spin systems that the chemical shifts of the $C^\beta H$ and $C^\gamma H$ protons are similar and sometimes degenerate. Consequently, it is often difficult to locate the $C^\beta H$–$C^\gamma H$ connectivities unambiguously in the HCCH-COSY spectrum. These problems are even further exacerbated for longer side-chain spin systems such as Arg, Pro, and Lys. The same problem presents itself in the interpretation of regular 2D ^1H–^1H COSY type spectra and can be circumvented by means of experiments that detect not only direct but relayed through-bond connectivities, for example, relayed COSY and HOHAHA/TOCSY spectroscopy. Similarly, the ambiguities present for longer side-chain spin systems in the HCCH-COSY experiment can be resolved unambiguously by recording an HCCH-TOCSY experiment in which carbon magnetization is transferred along the carbon chain by isotropic mixing.

In order to ensure that the HCCH-TOCSY experiment is recorded under conditions which are optimal for the observation of relayed connectivities, it is essential to consider in detail the expected theoretical cross-peak intensities as a function of isotropic mixing time. As discussed previously (Bax et al., 1990b), the DIPSI-3 sequence (Shaka et al., 1988) is ideally suited for isotropic mixing of ^{13}C magnetization. For the case of ^{13}C with relatively large homonuclear couplings (30–40 Hz), the DIPSI-3 sequence can cover a bandwidth of

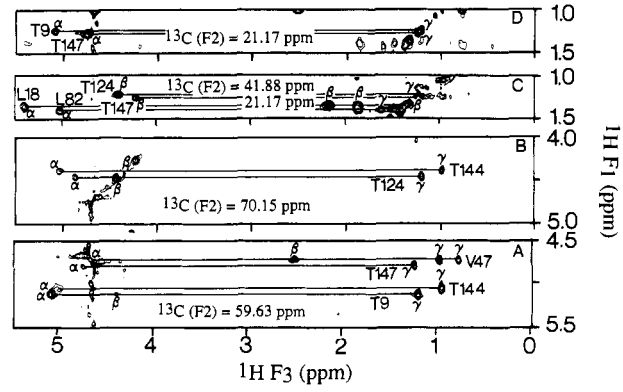

FIGURE 6: Selected slices at different $^{13}C(F_2)$ chemical shifts of the HCCH-TOCSY (first and fourth panels) and HCCH-COSY (second and third panels) spectra of uniformly $^{15}N/^{13}C$-labeled IL-1β principally illustrating Thr spin sysems. Note that the direct $C^\gamma H$–$C^\beta H$ and $C^\alpha H$–$C^\beta H$ cross-peaks for the threonine spin systems are either very weak or absent in the HCCH-TOCSY spectrum but are strong in the HCCH-COSY spectrum.

ca. $\pm 0.75\nu$, where ν is the strength of the applied ^{13}C rf field. Thus, on a 500-MHz spectrometer, an rf field strength of only ~7 kHz is needed for efficient isotropic mixing of the aliphatic resonances. On our inverse ^1H probe head, this requires 12.5 W of rf power, which is sufficiently low to permit mixing for

durations as long as 25 ms without causing substantial sample heating. The rate at which magnetization is transferred from one carbon to its neighbor depends on the size of the effective J coupling, J_{eff}, present during the mixing period. For coupled ^{13}C nuclei with widely different chemical shifts (e.g., Thr-Cβ and -Cγ), the effective J coupling can be substantially smaller than the real J coupling (Bax et al., 1990b). This results in a significant reduction in the rate of ^{13}C magnetization transfer which must be taken into account in simulations of the magnetization transfer process.

Figure 5 shows the calculated fraction of magnetization that is transferred from one carbon to another as a function of the length of the isotropic mixing period for various amino acids. These simulations employ approximate values for the effective J couplings that are smaller than the real J couplings (Tran-Dinh et al., 1974; Jogn et al., 1974; Krivdin & Kalabin, 1989). This apparent reduction depends on the difference between the ^{13}C shifts of the coupled ^{13}C resonances and was estimated with an rf field of 7 kHz and a ^{13}C frequency of 125.76 MHz (i.e., a 500-MHz spectrometer). It should be noted, however, that the general shape of these curves does not depend strongly on either the rf field or the magnetic field strength. In all the simulations, the presence of carbonyl or aromatic carbons has been neglected because the effective J coupling during isotropic mixing to the aliphatic carbon is very small (<10 Hz). In addition, for simplicity, the magnetization of all ^{13}C nuclei was assumed to relax at a rate of 33 s^{-1} during the isotropic mixing period. Because in-phase and antiphase magnetization components that participate in the magnetization transfer process relax at different rates, a proper calculation of the pertinent relaxation rates occurring during isotropic mixing is rather complex. The relaxation rate used for the simulation corresponds to the magnetization transfer pathway that results in cross-peaks, assuming a chain of methine carbons, tumbling isotropically with a correlation time of 10 ns and an order parameter S^2 of 0.85. In practice, of course, ^{13}C relaxation rates will vary over a substantial range, depending on the local order parameter (i.e., internal mobility) and on the number of protons attached to the ^{13}C nucleus. Thus, the curves shown in Figure 5 provide only an approximate, but very useful, guide of what magnetization transfer to expect for a given mixing time duration. Calculation of exact curves would require accurate knowledge of $^1J_{CC}$ couplings, ^{13}C chemical shifts, and longitudinal and transverse ^{13}C relaxation rates. Cross-peak intensities observed in the HCCH-TOCSY experiment are proportional to the amount of carbon–carbon magnetization transfer but are attenuated 2-fold if one of the carbons has two magnetically inequivalent protons attached and 4-fold if both carbons have nonequivalent protons attached.

For the simplest case of a two-spin system, transfer of magnetization from one carbon to its neighbor occurs in a cosinusoidal manner (Braunschweiler & Ernst, 1983), with a period of $1/J_{eff}$. For Ala, the Cα and Cβ resonances differ in chemical shift by ~33 ppm, and consequently, J_{eff} (25 Hz) is much smaller than the real $J_{C\alpha C\beta}$ coupling (35 Hz). For Ser, the difference in Cα and Cβ shifts is typically small (<10 ppm) so that the effective J coupling will be close to its normal value (37 Hz). As a result, magnetization transfer between the Cα and Cβ carbons occurs faster for Ser than for Ala residues (top left-hand panel in Figure 5). For other two-carbon systems (i.e., His, Phe, Tyr, Trp, Cys, Asp, and Asn) magnetization occurs at a rate that is intermediate between the Ala and Ser curves. Similarly, the $J_{C\alpha C\beta}$ coupling for Thr is close to its regular value as the Cα – Cβ chemical shift difference is typically less than 10 ppm, whereas the $J_{C\beta C\gamma}$ coupling is reduced by almost 50% because of the large Cβ – Cγ chemical shift difference (~50 ppm). Even though the carbon topology of the Thr side chain is the same as that for Glu, the reduction in the Thr $J_{C\beta C\gamma}$ coupling caused by offset effects makes the transfer of magnetization from the Cβ to the Cγ carbon considerably less efficient in Thr than in Glu, as is readily seen in Figure 5. The transfer efficiency shown for Glu also applies to Gln and Met.

The magnetization transfer efficiencies in Pro and Arg are also very similar, although transfer to the Cδ of Arg may often appear more intense than that for the Cδ of Pro due to the frequently observed increase in mobility at the end of the long Arg side chain. For both residues the effective $J_{C\alpha C\beta}$ coupling is significantly smaller than the real J coupling because of the large difference in Cα and Cβ chemical shifts. Note that if all one-bond J_{CC} couplings were identical, transfer from Cα to Cβ would follow the same curve as transfer from Cδ to Cγ and transfer from Cα to Cγ would be identical with transfer from Cδ to Cβ. For Lys, $J_{C\alpha C\beta}$ is expected to be only slightly smaller than the other one-bond couplings. Thus, transfer from Cϵ to Cδ (not shown) follows the same pattern as from Cα to Cβ, and so on.

The curves shown in Figure 5 are calculated for net magnetization transfer during the isotropic mixing period alone. In practice, however, dephasing of ^{13}C magnetization also occurs during the $\delta 1$ and $\delta 2$ periods (cf. the HCCH-TOCSY pulse scheme under Experimental Procedures). This has the effect of shifting the curves displayed in Figure 5 to the left by several milliseconds. In addition, J_{CC} dephasing occurs during the evolution period t_2. This also results in a left shift of the curves, but by a variable amount depending on the t_2 duration, and, in addition, causes F_2 line shapes to deviate slightly from the ideal absorptive phase.

From analysis of the theoretical curves shown in Figure 5, we concluded that an isotropic mixing time in the range 20–30 ms was optimal for the observation of relayed connectivities. Examples of different sorts of relayed connectivities observed in the 24-ms mixing time HCCH-TOCSY spectra are illustrated in Figures 6–10.

Figure 6 illustrates some Thr spin systems and affords a comparison of the HCCH-COSY and HCCH-TOCSY spectra. The top two panels in Figure 6 are taken at the same ^{13}C chemical shift of 21.17 ppm and illustrate the connectivities that are observed from the C$^\gamma$H proton of Thr in the 24-ms HCCH-TOCSY (first panel) and the HCCH-COSY (second panel) spectra. In the HCCH-COSY spectrum, a strong cross-peak corresponding to the direct connectivity to the C$^\beta$H proton is observed, while in the HCCH-TOCSY spectrum a strong cross-peak arises from the relayed C$^\gamma$H–C$^\alpha$H connectivity. As predicted from the simulations (Figure 5), the direct C$^\gamma$H–C$^\beta$H connectivity is not observed in the HCCH-TOCSY spectrum recorded with a 24-ms isotropic mixing time. In the case of Val, on the other hand, the intensities of the relayed C$^\gamma$H–C$^\alpha$H and direct C$^\gamma$H–C$^\beta$H cross-peaks are comparable and slightly weaker than that of the relayed C$^{\gamma a}$H–C$^{\gamma b}$H cross-peak between the two methyl carbons (cf. the theoretical curves in Figure 5 and the experimental data in the bottom panel of Figure 6 and the top two panels of Figure 9).

Figure 7 illustrates relayed connectivities originating from the C$^\alpha$H proton for a number of different amino acid spin systems in the 24-ms HCCH-TOCSY spectrum. Note that complete spin systems may be delineated not only for AM(PT)X spin systems such as Glu, Gln, and Met (see slices at 53.38, 55.03, 56.68, 57.99, and 58.65 ppm) but also for Val,

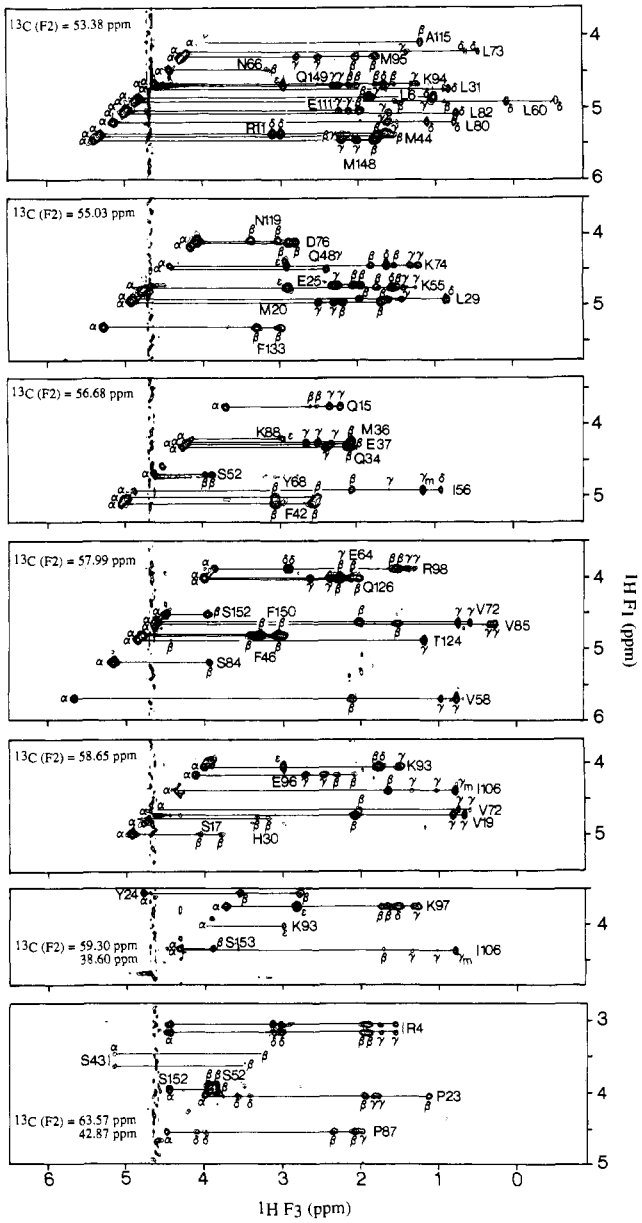

FIGURE 7: Selected slices at different $^{13}C(F_2)$ chemical shifts of the HCCH-TOCSY spectrum of uniformly $^{15}N/^{13}C$-labeled IL-1β illustrating relayed connectivities originating from the $C^{\alpha}H$ proton of several longer side chain amino acid spin systems such as Glu, Gln, Met, Pro, Arg, and Lys.

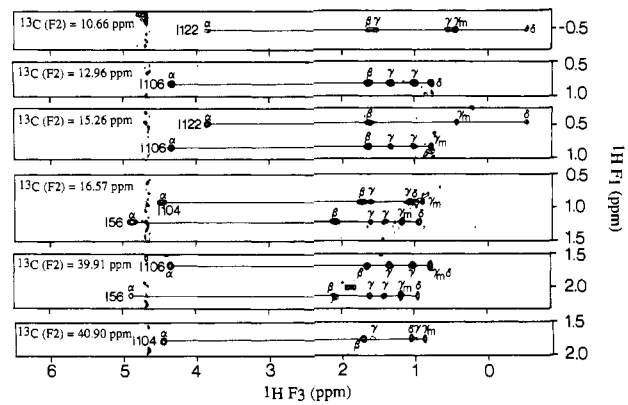

FIGURE 8: Selected slices at different $^{13}C(F_2)$ chemical shifts of the HCCH-TOCSY spectrum of uniformly $^{15}N/^{13}C$-labeled IL-1β illustrating multiple relayed connectivities originating from the $C^{\delta}H_3$, $C^{\gamma m}H_3$, and $C^{\beta}H$ protons of several Ile spin systems.

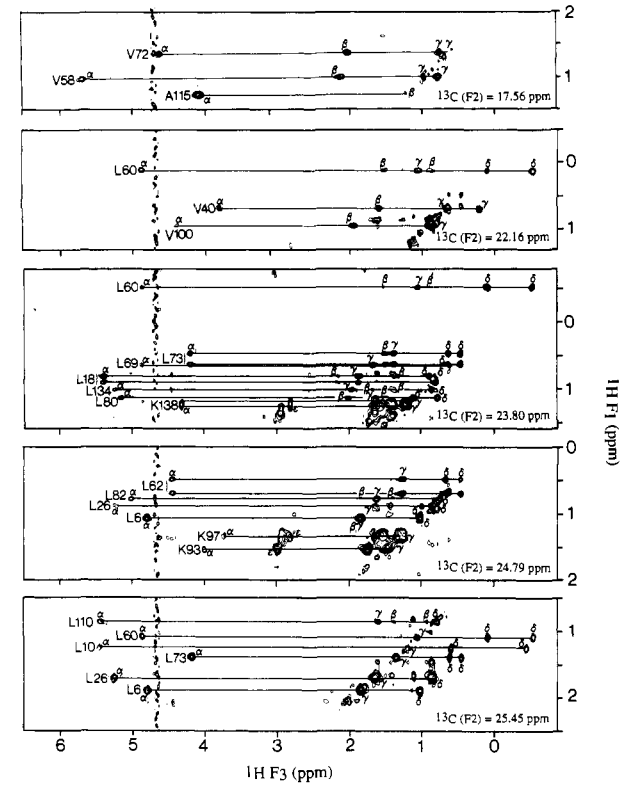

FIGURE 9: Selected slices at different $^{13}C(F_2)$ chemical shifts of the HCCH-TOCSY spectrum of uniformly $^{15}N/^{13}C$-labeled IL-1β illustrating multiple relayed connectivities originating from the $C^{\gamma}H_3$ protons of Val, the $C^{\delta}H_3$ and $C^{\gamma}H$ protons of Leu, and the $C^{\gamma}H$ protons of Lys.

Pro, Arg, and Lys. It should be noted, however, that the Cβ and Cγ chemical shifts of Met are very similar, and likewise, the difference in Cβ and Cγ chemical shift for Gln and Glu may be as small as 1 ppm (e.g., Glu-111 in Table I). Consequently, it is essential in these cases to verify the identification of the direct $C^{\alpha}H$–$C^{\beta}H$ connectivities with the HCCH-COSY experiment, even though the intensity of the $C^{\alpha}H$–$C^{\gamma}H$ cross-peaks is usually significantly stronger, and never weaker, than those of the direct $C^{\alpha}H$–$C^{\beta}H$ cross-peaks in the 24-ms HCCH-TOCSY spectrum. Examples of Val spin systems are evident at $\delta^{13}C$ = 57.99 ppm (Val-58 and Val-85) and $\delta^{13}C$ = 58.65 ppm (Val-19 and Val-72). In the case of the Val spin systems, the intensities of the direct $C^{\alpha}H$–$C^{\beta}H$ and relayed $C^{\alpha}H$–$C^{\gamma}H$ cross-peaks are comparable, although the latter tend to be slightly stronger because the $C^{\gamma}H$ proton resonance is narrower than the $C^{\beta}H$ one. Complete spin systems for several Leu residues (Leu-6, Leu-29, Leu-31, Leu-60, Leu-73, Leu-80, and Leu-82) may be seen in the slices at $\delta^{13}C$ = 53.38 and 55.03 ppm, and the intensities of the direct $C^{\alpha}H$–$C^{\beta}H$ and relayed $C^{\alpha}H$–$C^{\gamma}H$ and $C^{\alpha}H$–$C^{\delta}H$ cross-peaks are usually comparable, as expected for a mixing time of 24 ms from the theoretical curves in Figure 5. Two Ile residues at $\delta^{13}C$ = 56.68 ppm (Ile-56) and $\delta^{13}C$ = 58.65-59.30 ppm (Ile-106; note that the $C^{\gamma m}H$ and $C^{\delta}H$ methyl resonances are superimposed) are also present in Figure 7. For this spin system, the ratio of cross-peak intensities tends to follow the pattern $C^{\alpha}H$–$C^{\gamma m}H$ > $C^{\alpha}H$–$C^{\delta}H$ ~ $C^{\alpha}H$–$C^{\beta}H$ > $C^{\alpha}H$–$C^{\gamma}H$. Although the latter cross-peaks are weak, they are still clearly detectable, which is rarely the case in conventional ^1H–^1H 2D HOHAHA spectra of much smaller proteins of 40–60 residues.

As discussed above in relation to the theoretical simulations, the behavior of Pro and Arg spin systems in the HCCH-TOCSY spectrum should be similar, with the proviso that connectivities to the $C^{\delta}H$ proton of arginine would be expected

Table I: ^{1}H and ^{13}C Assignments for Uniformly $^{15}N/^{13}C$-Labeled IL-1β at 36 °C and pH 5.4[a]

Gly

	G22 Cα	G33 Cα	G49 Cα	G61 Cα
^{1}H	4.12,3.97	3.99,3.77	4.12,3.94	4.15,2.38
^{13}C	43.85	46.33	44.51	42.05
	G135 Cα	G136 Cα	G139 Cα	G140 Cα
^{1}H	4.92,4.02	3.84,2.93	4.02,3.83	4.20,3.78
^{13}C	44.68	44.02	45.00	44.35

Ala

	A1		A28		A115		A59	
	Cα	Cβ	Cα	Cβ	Cα	Cβ	Cα	Cβ
^{1}H	4.36	1.47	6.16	1.31	4.05	1.17	5.42	1.51
^{13}C	50.26	17.23	49.95	21.33	53.06	17.72	50.26	22.65

	A127	
	Cα	Cβ
^{1}H	4.38	1.44
^{13}C	50.92	19.20

Ser

	S5		S13		S17		S21	
	Cα	Cβ	Cα	Cβ	Cα	Cβ	Cα	Cβ
^{1}H	5.67	3.68,3.55	3.99	3.95,3.65	4.91	4.03,3.76	4.52	3.60,3.52
^{13}C	56.34	65.55	59.79	61.61	58.47	65.05	56.18	62.59
	S43		S45		S52		S70	
	Cα	Cβ	Cα	Cβ	Cα	Cβ	Cα	Cβ
^{1}H	5.16	3.61,3.45	5.36	3.71,3.58	4.63	3.97,3.88	5.23	3.66,3.28
^{13}C	55.85	63.08	56.35	64.72	56.84	63.74	55.19	66.70
	S84		S114		S123		S125	
	Cα	Cβ	Cα	Cβ	Cα	Cβ	Cα	Cβ
^{1}H	5.15	3.92,3.90	3.90	4.37,4.10	5.82	3.00,2.06	4.97	3.98,3.93
13C	57.82	63.08	58.65	62.59	57.00	66.87	56.18	63.74
	S152		S153					
	Cα	Cβ	Cα	Cβ				
^{1}H	4.48	3.94,3.94	4.31	3.89,3.89				
^{13}C	57.82	63.41	59.14	64.40				

Asn/Asp

	N7		D12		D35		N53	
	Cα	Cβ	Cα	Cβ	Cα	Cβ	Cα	Cβ
^{1}H	6.25	2.86,2.32	4.65	2.69,2.28	4.75	2.89,2.79	4.60	2.90,2.83
^{13}C	51.25	38.92	52.73	40.40	54.53	40.40	53.87	37.77
	D54		N66		D75		D76	
	Cα	Cβ	Cα	Cβ	Cα	Cβ	Cα	Cβ
^{1}H	4.59	2.77,2.77	4.41	3.14,3.01	4.15	2.81,2.66	4.07	2.86,2.79
^{13}C	53.87	40.07	53.39	36.29	55.19	38.75	55.03	39.58
	D86		N89		N102		N107	
	Cα	Cβ	Cα	Cβ	Cα	Cβ	Cα	Cβ
^{1}H	4.90	2.96,2.69	4.75	2.64,2.59	5.01	2.92,2.29	4.27	2.99,2.72
^{13}C	50.59	41.55	52.40	40.73	51.91	38.92	53.87	36.45
	N108		N119		N129		D142	
	Cα	Cβ	Cα	Cβ	Cα	Cβ	Cα	Cβ
^{1}H	4.38	3.02,3.02	4.04	3.37,3.03	4.18	3.31,2.55	4.93	2.82,2.57
^{13}C	54.21	37.11	54.86	37.44	53.87	37.44	53.55	41.06

	D145	
	Cα	Cβ
^{1}H	5.58	2.54,2.42
^{13}C	52.23	42.70

Cys

	C8		C71	
	Cα	Cβ	Cα	Cβ
^{1}H	5.76	2.96,2.86	5.53	2.86,2.46
^{13}C	55.19	32.35	56.02	29.72

His

	H30	
	Cα	Cβ
^{1}H	4.69	3.23,3.16
^{13}C	58.81	27.25

Tyr

	Y24				Y68			
	Cα	Cβ	Cδ	Cε	Cα	Cβ	Cδ	Cε
^{1}H	4.78	3.54,2.76	7.09	6.78	4.96	3.08,2.51	6.88	6.51
^{13}C	55.36	38.76	133.14	117.32	56.84	42.54	132.16	116.50
	Y90				Y121			
	Cα	Cβ	Cδ	Cε	Cα	Cβ	Cδ	Cε
^{1}H	4.19	2.50,2.30	6.74	6.63	5.64	3.50,2.41	7.01	6.63
^{13}C	55.69	40.89	132.16	117.48	56.02	41.39	132.65	117.32

Phe

			F42					F46		
	Cα	Cβ	Cδ	Cε	Cζ	Cα	Cβ	Cδ	Cε	Cζ
^{1}H	5.04	3.07,2.57	6.90	7.00	6.62	4.77	3.37,2.98	7.23	7.13	7.23
^{13}C	56.68	40.56	130.69	130.20	127.43	58.15	37.44	131.50	129.87	128.74
			F99					F101		
	Cα	Cβ	Cδ	Cε	Cζ	Cα	Cβ	Cδ	Cε	Cζ
^{1}H	5.16	3.69,2.87	7.51	7.04	6.89	5.15	2.70,2.67	6.98	7.06	6.81
^{13}C	57.16	40.73	131.02	130.53	129.22	55.36	41.88	130.85	130.37	128.74
			F112					F117		
	Cα	Cβ	Cδ	Cε	Cζ	Cα	Cβ	Cδ	Cε	Cζ
^{1}H	5.23	2.54,2.36	6.62	6.65	6.63	4.86	2.64,2.58	6.91	6.81	6.91
^{13}C	55.69	41.23	130.53	130.53	129.22	52.89	38.27	132.16	129.87	128.41
			F133					F146		
	Cα	Cβ	Cδ	Cε	Cζ	Cα	Cβ	Cδ	Cε	Cζ
^{1}H	5.27	3.30,2.97	7.31	7.23	7.13	5.22	3.09,2.63	7.01	7.11	6.81
^{13}C	54.86	41.55	133.14	130.20	129.22	55.69	43.69	130.85	130.37	128.74
			F150							
	Cα	Cβ	Cδ	Cε	Cζ					
^{1}H	4.77	3.26,3.03	7.33	7.39	7.39					
^{13}C	57.82	38.76	130.85	130.85	129.06					

Trp

	W120					
	Cα	Cβ	Cζ2	Cη2	Cζ3	Cε3	Cδ1
^{1}H	4.98	3.67,2.92	7.45	7.21	7.21	7.10	7.30
^{13}C	56.51	28.73	113.73	123.84	121.24	118.95	

Met

	M20			M36			M44		
	Cα	Cβ	Cγ	Cα	Cβ	Cγ	Cα	Cβ	Cγ
^{1}H	4.90	2.19,1.70	2.50,2.30	4.21	2.05,2.05	2.69,2.53	5.30	2.23,1.56	2.23,2.23
^{13}C	54.86	31.85	31.85	56.84	31.36	30.87	53.55	34.81	34.32
	M95			M130			M148		
	Cα	Cβ	Cγ	Cα	Cβ	Cγ	Cα	Cβ	Cγ
^{1}H	4.23	2.00,1.76	2.75,2.50	5.23	2.36,2.15	2.72,2.36	5.39	1.78,1.78	2.21,2.00
^{13}C	53.39	33.67	32.68	51.58	31.36	32.02	53.22	36.78	31.20

Glu/Gln

	Q14			Q15			E25		
	Cα	Cβ	Cγ	Cα	Cβ	Cγ	Cα	Cβ	Cγ
^{1}H	4.55	2.56,1.59	2.36,2.36	3.55	2.62,2.53	2.39,2.25	4.67	2.04,1.94	2.30,2.24
^{13}C	54.37	27.91	33.50	56.68	24.62	33.01	55.19	33.83	36.45
	Q32			Q34			E37		
	Cα	Cβ	Cγ	Cα	Cβ	Cγ	Cα	Cβ	Cγ
^{1}H	4.53	2.19,1.98	2.31,2.25	4.27	2.10,2.10	2.42	4.22	2.10,2.02	2.36,2.36
^{13}C	54.21	30.20	32.84	56.51	27.58	33.01	57.16	28.57	35.31
	Q38			Q39			Q48		
	Cα	Cβ	Cγ	Cα	Cβ	Cγ	Cα	Cβ	Cγ
^{1}H	4.21	2.23,1.97	2.50,2.40	4.42	2.30,2.03	2.56,2.42	4.44	2.08,1.97	2.42,2.42
^{13}C	55.52	29.06	33.67	55.85	29.22	33.99	55.36	29.06	33.34
	E50			E51			E64		
	Cα	Cβ	Cγ	Cα	Cβ	Cγ	Cα	Cβ	Cγ
^{1}H	4.35	2.06,1.92	2.25,2.25	4.50	2.11,2.01	2.34,2.27	3.98	2.24,2.09	2.24,2.24
^{13}C	55.85	29.22	35.64	55.52	30.21	35.64	57.82	27.91	33.34
	Q81			E83			E96		
	Cα	Cβ	Cγ	Cα	Cβ	Cγ	Cα	Cβ	Cγ
^{1}H	4.98	2.11,2.11	2.69,2.51	4.63	2.10,1.95	2.31,2.31	4.09	2.23,2.08	2.73,2.44
^{13}C	53.06	31.69	32.18	54.05	32.84	36.62	58.65	28.08	36.95
	E105			E111			E113		
	Cα	Cβ	Cγ	Cα	Cβ	Cγ	Cα	Cβ	Cγ
^{1}H	5.14	1.94,1.73	2.14,2.05	5.00	1.99,1.99	2.22,2.11	4.47	1.42,1.42	2.66,2.56
^{13}C	54.21	30.54	35.47	53.06	31.52	32.35	53.87	28.73	33.99
	Q116			Q126			E128		
	Cα	Cβ	Cγ	Cα	Cβ	Cγ	Cα	Cβ	Cγ
^{1}H	3.61	1.42,0.98	1.31,0.72	3.98	2.24,2.01	2.63,2.38	4.04	2.27,1.96	2.56,2.50
^{13}C	56.02	28.73	32.35	57.66	28.24	33.34	53.52	30.71	34.32
	Q141			Q149					
	Cα	Cβ	Cγ	Cα	Cβ	Cγ			
^{1}H	4.29	2.20,2.00	2.39,2.39	4.63	2.07,1.99	2.31,2.25			
^{13}C	55.85	28.89	33.01	53.55	29.55	33.67			

Thr

	T9			T79			T124		
	Cα	Cβ	Cγ	Cα	Cβ	Cγ	Cα	Cβ	Cγ
^{1}H	5.06	4.39	1.18	4.58	3.93	1.20	4.83	4.39	1.16
^{13}C	59.30	71.47	21.01	61.60	72.28	20.35	57.99	70.31	21.01
	T137			T144			T147		
	Cα	Cβ	Cγ	Cα	Cβ	Cγ	Cα	Cβ	Cγ
^{1}H	4.31	3.99	0.96	4.99	4.39	0.96	4.74	4.19	1.22
^{13}C	59.63	70.15	20.52	59.96	70.81	21.33	60.78	69.65	20.52

Val

	V3			V19			V40		
	Cα	Cβ	Cγ	Cα	Cβ	Cγ	Cα	Cβ	Cγ
^{1}H	4.25	1.93	0.83,0.83	4.68	2.03	0.78,0.66	3.78	1.58	0.62,0.19
^{13}C	60.95	32.68	20.68,21.88	58.46	35.60	21.50,19.50	61.60	32.00	19.50,20.80
	V41			V47			V58		
	Cα	Cβ	Cγ	Cα	Cβ	Cγ	Cα	Cβ	Cγ
^{1}H	4.24	1.83	0.85,0.85	4.66	2.51	0.95,0.73	5.64	2.08	0.82,0.73
^{13}C	61.30	32.35	21.50,20.50	59.79	32.70	21.50,18.87	57.99	36.62	17.89,21.20
	V72			V85			V100		
	Cα	Cβ	Cγ	Cα	Cβ	Cγ	Cα	Cβ	Cγ
^{1}H	4.58	1.99	0.71,0.55	4.59	1.52	0.33,0.25	4.36	1.92	0.90,0.82
^{13}C	57.99	35.60	20.68,17.76	57.66	34.46	17.89,19.86	62.90	31.69	22.49,20.85
	V132			V151					
	Cα	Cβ	Cγ	Cα	Cβ	Cγ			
^{1}H	4.42	1.75	0.86,0.86	4.36	1.84	0.95,0.90			
^{13}C	62.26	31.69	22.82,20.52	60.90	33.00	22.16,20.66			

Leu

	L6				L10			
	Cα	Cβ	Cγ	Cδ	Cα	Cβ	Cγ	Cδ
^{1}H	4.78	1.82,1.81	1.84	1.02,0.98	5.45	1.53,1.07	1.18	0.58,-0.40
^{13}C	53.39	45.00	26.10	25.28,25.28	53.06	46.31	26.43	23.15,22.82
	L18				L26			
	Cα	Cβ	Cγ	Cδ	Cα	Cβ	Cγ	Cδ
^{1}H	5.38	2.15,1.40	1.86	0.89,0.77	5.24	1.63,1.42	1.63	0.89,0.83
^{13}C	53.88	42.04	28.24	23.96,23.96	52.56	45.00	25.78	24.60,24.60
	L29				L31			
	Cα	Cβ	Cγ	Cδ	Cα	Cβ	Cγ	Cδ
^{1}H	4.87	1.95,1.58	1.42	0.86,0.83	4.67	1.68,1.25	1.64	0.89,0.83
^{13}C	54.86	43.86	27.09	25.61,25.61	53.06	44.34	25.78	25.78,25.78
	L60				L62			
	Cα	Cβ	Cγ	Cδ	Cα	Cβ	Cγ	Cδ
^{1}H	4.86	1.50,0.86	1.03	0.08,-0.56	4.46	1.42,1.36	1.25	0.64,0.44
^{13}C	53.06	44.84	26.10	22.81,23.80	53.72	40.24	28.24	24.85,24.85
	L67				L69			
	Cα	Cβ	Cγ	Cδ	Cα	Cβ	Cγ	Cδ
^{1}H	5.34	1.42,1.17	1.61	0.89,0.89	4.84	2.00,1.69	1.69	0.67,0.67
^{13}C	52.56	47.47	22.45	25.78,25.78	56.02	44.67	28.56	23.96,23.96
	L73				L80			
	Cα	Cβ	Cγ	Cδ	Cα	Cβ	Cγ	Cδ
^{1}H	4.17	1.48,1.36	1.35	0.59,0.43	5.13	2.00,1.50	1.60,1.09,0.75	
^{13}C	53.72	42.36	26.26	23.63,23.63	53.39	43.86	26.43	23.80,25.61
	L82				L110			
	Cα	Cβ	Cγ	Cδ	Cα	Cβ	Cγ	Cδ
^{1}H	5.01	1.86,1.39	1.61	0.75,0.75	5.42	1.36,0.94	1.54	0.77,0.73
^{13}C	53.72	42.04	28.22	24.46,24.46	53.06	45.17	26.76	25.94 24.13
	L134							
	Cα	Cβ	Cγ	Cδ				
^{1}H	5.24	1.89,1.67	1.97	1.00,0.89				
^{13}C	53.06	43.36	27.58	24.13,24.29				

Ile

	I56				I104			
	Cα	Cβ	Cγm	Cγ	Cδ	Cα	Cβ	Cγm	Cγ	Cδ
^{1}H	4.86	2.09	1.16	1.61,1.39	0.93	4.45	1.74	0.90	1.61,1.00	1.07
^{13}C	56.50	39.91	16.57	26.76	11.64	59.96	40.89	16.90	27.25	11.64
	I106					I122				
	Cα	Cβ	Cγm	Cγ	Cδ	Cα	Cβ	Cγm	Cγ	Cδ
^{1}H	4.33	1.68	0.80	1.36,1.03	0.78	3.84	1.62	0.41	1.50,0.50	-0.49
^{13}C	58.64	39.91	15.59	27.09	12.96	65.60	36.29	15.59	28.08	10.82
	I143									
	Cα	Cβ	Cγm	Cγ	Cδ					
^{1}H	4.00	2.53	0.78	2.42,1.39	0.53					
^{13}C	61.28	35.97	18.87	27.08	13.28					

Pro

	P2				P2*[b]			
	Cα	Cβ	Cγ	Cδ	Cα	Cβ	Cγ	Cδ
^{1}H	4.50	2.31,1.89	2.00,2.00	3.68,3.59	4.50	2.45,2.00	2.05,2.00	3.43,3.38
^{13}C	62.42	31.69	26.76	49.93	61.44	32.18	25.78	48.79
	P23				P57			
	Cα	Cβ	Cγ	Cδ	Cα	Cβ	Cγ	Cδ
^{1}H	4.02	1.97,1.14	1.86,1.77	3.59,3.44	5.37	2.15,1.83	2/24,1.86	4.05,3.96
^{13}C	63.58	31.20	26.43	48.46	61.93	31.36	26.76	51.09
	P78				P87			
	Cα	Cβ	Cγ	Cδ	Cα	Cβ	Cγ	Cδ
^{1}H	3.19	0.31,0.19	0.03,-0.29	3.06,2.08	4.52	2.36,2.08	2.05,1.99	4.18,4.05
^{13}C	62.92	31.04	26.01	50.47	63.58	31.69	26.69	50.76
	P91				P118			
	Cα	Cβ	Cγ	Cδ	Cα	Cβ	Cγ	Cδ
^{1}H	4.25	2.32,1.92	1.94,1.67	3.67,2.44	4.40	2.29,1.78	2.00,1.87	3.54,3.31
^{13}C	62.26	33.67	24.21	49.27	62.92	31.69	27.09	49.44
	P131							
	Cα	Cβ	Cγ	Cδ				
^{1}H	5.20	2.53,1.95	2.17,2.00	4.02,3.78				
^{13}C	62.26	32.35	27.75	50.43				

Table I (Continued)

Arg

	R4 Cα	Cβ	Cγ	Cδ	R11 Cα	Cβ	Cγ	Cδ
^1H	4.50	2.00,1.94	1.77,1.58	3.17,3.06	5.31	1.64,1.64	1.67,1.67	3.08,3.00
^{13}C	55.69	30.71	27.09	42.70	53.54	34.15	26.92	43.36

	R98 Cα	Cβ	Cγ	Cδ
^1H	3.89	1.42,1.33	1.58,1.53	2.97,2.92
^{13}C	58.15	32.35	29.06	41.23

Lys

	K16 Cα	Cβ	Cγ	Cδ	Cε
^1H	3.66	2.00,0.93	1.24,1.38	2.00,1.24	2.65,2.65
^{13}C	58.32	29.92			41.23

	K27 Cα	Cβ	Cγ	Cδ	Cε
^1H	5.17	1.89,1.49	1.19,1.00	1.49,1.49	2.78,.278
^{13}C	54.53	36.95	24.86	29.06	41.71

	K55 Cα	Cβ	Cγ	Cδ	Cε
^1H	4.72	1.78,1.50	1.44,1.27	1.58,1.58	2.92,2.92
^{13}C	54.86	33.99	24.29	29.06	41.23

	K63 Cα	Cβ	Cγ	Cδ	Cε
^1H	3.84	-	-	-	-
^{13}C	-	-	-	-	-

	K65 Cα	Cβ	Cγ	Cδ	Cε
^1H	4.48	1.77,1.42	1.00,0.81	1.42,1.36	3.00,3.00
^{13}C	54.21	34.32	23.80	29.06	41.39

	K74 Cα	Cβ	Cγ	Cδ	Cε
^1H	4.42	1.86,1.56	1.33,1.22	1.67,1.67	2.94,2.94
^{13}C	55.00	33.50	24.46	28.57	40.90

	K77 Cα	Cβ	Cγ	Cδ	Cε
^1H	4.66	1.67,1.60	1.39,1.39	1.78,1.78	3.17,3.17
^{13}C	52.56	33.99	23.31	28.56	41.23

	K88 Cα	Cβ	Cγ	Cδ	Cε
^1H	4.24	1.83,1.72	1.47,1.47	1.72,1.72	3.03,3.03
^{13}C	57.16	31.52	24.29	28.41	41.06

	K92 Cα	Cβ	Cγ	Cδ	Cε
^1H	4.42	1.64,1.64	-	-	2.97,2.97
^{13}C	55.03	-	-	-	-

	K93 Cα	Cβ	Cγ	Cδ	Cε
^1H	4.00	1.75,1.75	1.53,1.47	1.75,1.75	3.00,3.00
^{13}C	58.80	32.18	24.62	28.56	41.06

	K94 Cα	Cβ	Cγ	Cδ	Cε
^1H	4.61	1.78,1.56	1.33,1.25	1.67,1.67	2.96,2.96
^{13}C	53.72	33.99	24.46	28.73	41.71

	K97 Cα	Cβ	Cγ	Cδ	Cε
^1H	3.75	1.75,1.65	1.53,1.53	1.33,1.26	2.83,2.83
^{13}C	59.13	31.85	24.61	28.24	41.06

	K103 Cα	Cβ	Cγ	Cδ	Cε
^1H	4.64	-	-	-	-
^{13}C	55.52	-	-	-	-

	K109 Cα	Cβ	Cγ	Cδ	Cε
^1H	4.81	1.94,1.86	1.47,1.39	1.64,1.47	2.97,2.97
^{13}C	54.15	34.71	24.46	28.24	41.23

	K138 Cα	Cβ	Cγ	Cδ	Cε
^1H	4.32	1.63,1.63	1.24,1.19	1.47,1.39	2.81,2.81
^{13}C	55.52	32.35	23.96	28.24	41.06

[a] ^1H and ^{13}C chemical shifts are reported relative to 3-(trimethylsilyl)propionic-d_4 acid. [b] There are two sets of chemical shifts for Pro-2 corresponding to the N-terminal Ala-1 and the des-Ala-1 forms of IL-1β (Driscoll et al., 1990a). P2* refers to the des-Ala-1 form.

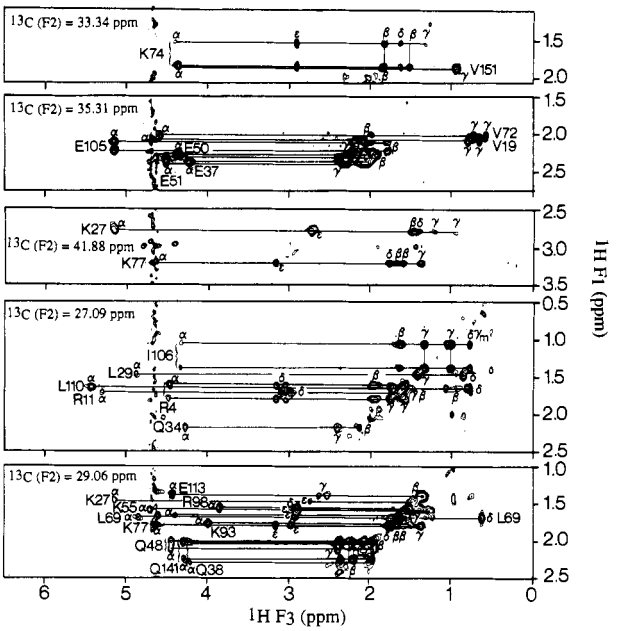

FIGURE 10: Selected slices at different $^{13}C(F_2)$ chemical shifts of the HCCH-TOCSY spectrum of uniformly $^{15}N/^{13}C$-labeled IL-1β illustrating connectivities originating from the C$^\beta$H and C$^\gamma$H protons of Glu and Gln, the C$^\gamma$H protons of Arg, the C$^\beta$H, C$^\delta$H, and C$^\epsilon$H protons of Lys, and the C$^\gamma$H protons of Ile.

to be significantly enhanced for exterior side chains due to an increase in mobility as one proceeds outward along the Arg side chain. In contrast, intensities of cross-peaks to the C$^\delta$H of proline would be expected to be reduced on account of the motional restrictions imposed by the five-membered proline ring. This is indeed what is observed: the C$^\alpha$H–C$^\delta$H connectivity for Arg-98 at $\delta^{13}C$ = 57.99 ppm is clearly stronger than the C$^\alpha$H–C$^\beta$H and C$^\alpha$H–C$^\gamma$H cross-peaks, while for Pro-23 and Pro-87 at $\delta^{13}C$ = 63.57 ppm the C$^\alpha$H–C$^\delta$H cross-peak intensities are comparable or weaker than the other two. In the same slice as these two Pro residues, one can also see the complete Arg-4 spin system originating from the C$^\delta$H protons at $\delta^{13}C$ = 42.87 ppm, with cross-peak intensities following a characteristic order, C$^\delta$H–C$^\alpha$H > C$^\delta$H–C$^\gamma$H ~ C$^\delta$H–C$^\beta$H, in agreement with theoretical expectations (Figure 5). Finally, complete Lys spin systems originating from the C$^\alpha$H proton are also clearly seen in Figure 7 (cf. Lys-94 at $\delta^{13}C$ = 53.38 ppm, Lys-55 and Lys-74 at $\delta^{13}C$ = 55.03 ppm, Lys-93 at $\delta^{13}C$ = 58.65 ppm, and Lys-97 at $\delta^{13}C$ = 59.30 ppm). Note how easily the C$^\alpha$H–C$^\epsilon$H, C$^\alpha$H–C$^\delta$H, and C$^\alpha$H–C$^\gamma$H relayed cross-peaks are observed. In this respect it is worth pointing out that, even in small proteins of 40–60 residues, it is rare to be able to delineate complete lysine, arginine, and proline spin systems originating from the C$^\alpha$H proton by use of conventional 2D ^1H–^1H HOHAHA spectroscopy, as even there the ratios of line widths to ^1H–^1H three-bond couplings are unfavorable for efficient magnetization transfer.

As already noted, the interpretation of the HCCH-COSY and HCCH-TOCSY spectra is rendered essentially foolproof through extensive cross-checks afforded by examining the connectivities between ^1H resonances observed at all the corresponding ^{13}C shifts of the directly bonded ^{13}C nuclei. This procedure is illustrated in Figure 8, which shows a series of relayed connectivities originating from the C$^\delta$H (10.66 and 12.96 ppm), C$^{\gamma m}$H (15.26 and 16.57 ppm), and C$^\beta$H (39.91 and 40.90 ppm) of four Ile residues (Ile-56, -104, -106, and -122). In virtually every case, the complete Ile spin system is identified from each of these starting points, thus confirming the ^1H assignments derived from the connectivities originating at the C$^\alpha$H protons and providing the ^{13}C chemical shifts of the other carbon atoms. It is worth pointing out here too that while in small proteins the C$^\beta$H and C$^{\gamma m}$H resonances are relatively easily identified in 2D ^1H–^1H COSY and HOHAHA spectra, connectivities to the C$^\gamma$H and C$^\delta$H resonances are often difficult to observe owing to large unresolved multiplet widths of the C$^\gamma$H resonances. In the HCCH-TOCSY spectrum, however, assignment of these protons is a simple matter.

A similar series of connectivities for Leu residues originating from the C$^\delta$H methyl (slices at $\delta^{13}C$ = 22.16, 23.80, and 24.79 ppm) and C$^\gamma$H protons (slice at $\delta^{13}C$ = 25.45 ppm) is shown in Figure 9. It may be noticed that the C$^\delta$H to C$^\beta$H relayed peaks and the direct C$^\gamma$H–C$^\beta$H peaks tend to be rather weak and sometimes even absent, in complete agreement with the simulations shown in Figure 5, so that the HCCH-COSY experiment (or alternatively a short 8–10-ms mixing time

HCCH-TOCSY experiment) still has a valuable role to play in confirming the identification of the Leu $C^{\beta}H$ resonance positions.

Finally, a number of connectivities originating successively from the $C^{\beta}H$ ($\delta^{13}C$ = 33.34 ppm), $C^{\delta}H$ ($\delta^{13}C$ = 29.06 ppm), and $C^{\epsilon}H$ ($\delta^{13}C$ = 41.88 ppm) protons of Lys and from the $C^{\gamma}H$ proton of Arg ($\delta^{13}C$ = 27.09 and 29.06 ppm) and the $C^{\gamma}H$ protons of Glu ($\delta^{13}C$ = 35.31 ppm) are shown in Figure 10. As in the previous examples, complete or virtually complete spin systems can be delineated starting from the different-side chain protons, thereby providing multiple checks on the assignments.

It is clear from the above examples that the combined use of the 3D HCCH-COSY and HCCH-TOCSY spectra provides a very powerful means for the unambiguous assignment of both the ^1H and ^{13}C chemical shifts of the side-chain protons and carbons. Using these spectra, we were able to obtain complete ^1H and ^{13}C assignments for the aliphatic side chains of all residues with the exception of only four lysine residues (Lys-16, Lys-63, Lys-92, and Lys-103) for which partial assignments were obtained. A complete list of assignments is provided in Table I.

The absence of complete connectivities for four of the lysine residues may be due to multiple side-chain conformations or to line broadening reducing the efficiency of magnetization transfer. Line broadening may arise from conformational restriction of lysine side-chain positions (cf. the lysine residue in the bottom panel of Figure 4 with nonequivalent $C^{\delta}H$ as well as $C^{\epsilon}H$ resonances, which additionally attenuates cross-peak intensities) or from an intermediate exchange process. The latter may well be the case for Lys-63 as the ^{15}N line width of the backbone amide group of this residue is extensively broadened by a chemical exchange contribution to T_2 (Clore et al., 1990b).

For completeness we have also included in Table I the ^1H chemical shifts of the aromatic protons together with the ^{13}C shifts of their directly bonded carbons. The ^1H aromatic spin systems had previously been delineated by 2D ^1H–^1H correlation methods (P.COSY and HOHAHA) and sequence specifically assigned from the observation of characteristic intraresidue NOEs from the aromatic ring protons to the NH, $C^{\alpha}H$, and $C^{\beta}H$ protons (Driscoll et al., 1990a). With these assignments in hand, the assignments of the ^{13}C shifts of the aromatic carbons attached to protons involved in intraaromatic NOEs could be obtained in a trivial manner from a 3D ^1H–^{13}C NOESY-HMQC spectrum (data not shown). The latter experiment was necessary as the present HCCH-COSY and HCCH-TOCSY experiments in which the carbon carrier was placed at 43 ppm could not be used to detect correlations involving aromatic carbons owing to the fact that the aromatic carbons resonate at the downfield end of the ^{13}C spectrum at ~130 ppm. As a result, adequate refocusing of ^{13}C chemical shifts of aromatic carbons by the ^{13}C 180° pulses before and after the ^{13}C 90° COSY mixing pulse was not obtained in the case of the HCCH-COSY experiment (cf. pulse sequence under Experimental Procedures), and the rf field strength used in the HCCH-TOCSY experiment was too weak to permit efficient isotropic mixing of the aromatic carbons.

The aliphatic ^{13}C side-chain assignments provided in Table I provide a reasonably large and comprehensive database of ^{13}C chemical shifts in proteins and expand on the previously available data on isolated amino acids and small peptides (Levy & Nelson, 1972; Howarth & Lilley, 1978) and the partial assignments recently obtained for staphylococcal nuclease by 2D heteronuclear methods (Wang et al., 1990). The distribution of ^{13}C aliphatic chemical shifts in IL-1β for the different amino acid residues is summarized graphically in Figure 11. The chemical shifts are comparable to those established for isolated amino acids and small peptides, but not surprisingly, the ranges for each carbon type are significantly larger. The information provided in Figure 11 may therefore serve as a useful aid in future assignment work. In general, chemical shifts are usually difficult to interpret. Nevertheless, empirical correlations may be of some use if treated with appropriate caution. For example, it has been noted in peptides that the Cα chemical shift of the residue preceding a proline is ~2 ppm upfield from its characteristic value (Torchia et al., 1975). There are eight prolines in IL-1β at positions 2, 23, 57, 78, 87, 91, 118, and 131. In five cases, the Cα chemical shift of the preceding residue (Ile-56, Lys-77, Asp-86, Phe-117, and Met-130) has the most upfield chemical shift in its residue class, while in another two (Ala-1 and Gly-22) the Cα chemical shift is clearly at the upfield end of its range. In the case of Tyr-90, which precedes Pro-91, there is no clear correlation. This, however, may have to do with the fact that the Tyr-90–Pro-91 peptide bond is in the cis conformation as evidenced from the observation of characteristic $C^{\alpha}H$–$C^{\alpha}H$ sequential NOEs between Tyr-90 and Pro-91 in the ^1H–^{13}C HMQC-NOESY spectrum, in agreement with the crystallographic findings for the X-ray structure of IL-1β (Finzel et al., 1989). The other proline residues, on the other hand, are all in the trans conformation as judged from both the NMR and X-ray data. In this regard, it is worth noting that, just as in the case of small peptides (Howarth & Lilley, 1978), the Cβ and Cγ chemical shifts of the *cis*-proline at position 91 are about 1 ppm downfield and 2 ppm upfield, respectively, of the corresponding shifts for the *trans*-proline residues.

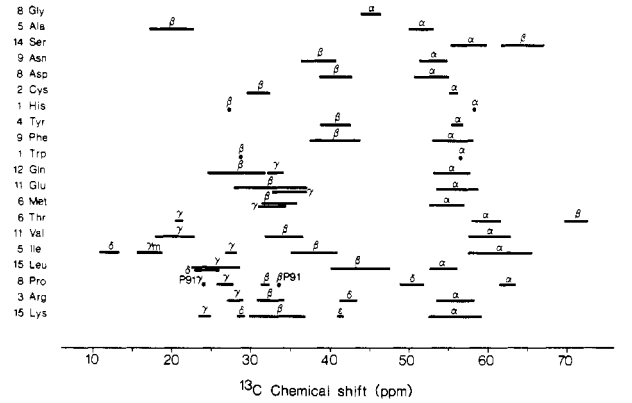

FIGURE 11: Summary of the ^{13}C chemical shift ranges observed for the different carbon atoms and different residue types in IL-1β. The number of residues present in IL-1β for each amino acid type is indicated at the left-hand side of the figure. In the case of the Pro residues, there are two sets of chemical shifts for Pro-2 corresponding to the N-terminal Ala-1 and des-Ala-1 forms of IL-1β (Driscoll et al., 1990a). Complete ^{13}C assignments were obtained for 11 out of the 15 lysine residues; no ^{13}C shifts were obtained for Lys-63, only $^{13}C\alpha$ shifts were obtained for Lys-92 and Lys-103, and only $^{13}C\alpha$, $^{13}C\beta$, and $^{13}C\epsilon$ shifts were obtained for Lys-16.

Concluding Remarks

The determination of protein structures in solution by NMR depends on the identification of a very large number of short (<5 Å) approximate interproton distance restraints derived from NOE measurements [see Wüthrich (1986, 1989), Clore and Gronenborn (1987, 1989), and Gronenborn and Clore (1990) for reviews]. A key requirement in this procedure involves not simply the assignment of the backbone ^1H resonances (NH and $C^{\alpha}H$) but equally importantly that of the side-chain resonances. Even for proteins of 50–100 residues,

it is often difficult to obtain complete side-chain assignments for long side chain amino acids such as Lys and Arg. This is not simply due to spectral overlap but to the relatively large ^1H line widths which render magnetization transfer through homonuclear ^1H–^1H couplings inefficient. Further, even when these assignments are made, extensive spectral overlap often precludes their use in the identification of NOESY cross-peaks. The data presented in this paper clearly show that 3D heteronuclear methods based on magnetization transfer via large one-bond ^1H–^{15}N, ^{15}N–^{13}C, ^1H–^{13}C, and ^{13}C–^{13}C couplings are highly efficient and sensitive even for molecules the size of IL-1β, which comprises 153 residues. In this respect we note that all the 3D spectra were recorded on a single 1.7 mM sample of uniformly $^{15}N/^{13}C$-labeled protein and the limiting factor in the duration of the experiments was not the signal-to-noise but the minimum number of phase cycles required to reduce spectral artifacts to an acceptable level. Indeed, all the 3D heteronuclear correlation spectra for the present paper were recorded in just 1 week of measuring time. Further, with the addition of a third dimension afforded by the ^{13}C nucleus, problems associated with extensive resonance overlap which are invariable present in the 2D ^1H–^1H and ^1H–^{13}C spectra of proteins the size of Il-1β are completely overcome.

To our knowledge, the ^1H, ^{15}N, and ^{13}C assignments of IL-1β provided by this paper and the preceding one (Driscoll et al., 1990a) represent the first example of a protein larger than 15 kDa for which essentially complete assignments of both backbone and side-chain resonances have been obtained by heteronuclear 3D NMR methods. Given that the attainable precision of a protein structure determination depends crucially on maximizing the number of approximate interproton distance restraints (Driscoll et al., 1989a,b; Kraulis et al., 1989), virtually complete assignments represent the necessary prerequisite in that endeavor. With the assignments for IL-1β firmly in hand, the way is now open for the full determination of a high-resolution 3D structure of Il-1β in solution by 3D ^1H–^{15}N and ^1H–^{13}C HMQC-NOESY spectroscopy, as well as 4D $^{13}C/^{15}N$ and $^{13}C/^{13}C$ edited NOESY spectroscopy (Kay et al., 1990c), at a precision comparable to the best that is now attainable for smaller proteins (Kraulis et al., 1989; Qian et al., 1989; Clore et al., 1990a).

ACKNOWLEDGMENTS

We thank Mark Payton for help with the fermentation, Lewis Kay and Mitsuhiko Ikura for useful discussions, Rolf Tschudin for assistance with the development of the spectrometer hardware, and Technic de Bouregas for kindly providing the program ANTIOPE for the computer simulations shown in Figure 5.

REFERENCES

Bax, A., Clore, G. M., Driscoll, P. C., Gronenborn, A. M., Ikura, M., & Kay, L. E. (1990a) *J. Magn. Reson. 87*, 620–627.

Bax, A., Clore, G. M., & Gronenborn, A. M. (1990b) *J. Magn. Reson. 88*, 425–431.

Braunschweiler, L., & Ernst, R. R. (1983) *J. Magn. Reson. 53*, 521–528.

Brühweiler, D., & Wagner, G. (1986) *J. Magn. Reson. 69*, 546–551.

Buell, G., Schulz, M.-F., Selzer, G., Chollet, A., Movva, R., Semon, D., Escanez, S., & Kawashima, E. (1985) *Nucleic Acids Res. 13*, 1923–1938.

Clore, G. M., & Gronenborn, A. M. (1987) *Protein Eng. 1*, 275–288.

Clore, G. M., & Gronenborn, A. M. (1989) *CRC Crit. Rev. Biochem. Mol. Biol. 24*, 479–564.

Clore, G. M., Appella, E., Yamada, M., Matsushima, K., & Gronenborn, A. M. (1990a) *Biochemistry 29*, 1689–1696.

Clore, G. M., Driscoll, P. C., Wingfield, P. T., & Gronenborn, A. M. (1990b) *Biochemistry 29*, 7387–7401.

Dinarello, C. A. (1988) *Ann. N.Y. Acad. Sci. 546*, 122–132.

Driscoll, P. C., Gronenborn, A. M., Beress, L., & Clore, G. M. (1989a) *Biochemistry 28*, 2188–2198.

Driscoll, P. ., Gronenborn, A. M., & Clore, G. M. (1989b) *FEBS Lett. 243*, 223–233.

Driscoll, P. C., Clore, G. M., Marion, D., Wingfield, P. T., & Gronenborn, A. M. (1990a) *Biochemistry 29*, 3542–3556.

Driscoll, P. C., Gronenborn, A. M., Wingfield, P. T., & Clore, G. M. (1990b) *Biochemistry 29*, 4668–4682.

Fesik, S. W., Eaton, H. L., Olejniczak, E. T., Zuiderweg, E. R. P., McIntosh, L. P., & Dahlquist, F. W. (1990) *J. Am. Chem. Soc. 112*, 886–887.

Finzel, B. C., Clancy, L. L., Holland, D. R., Muchmore, S. W., Watenpaugh, K. D., & Einspahr, H. M. (1989) *J. Mol. Biol. 209*, 779–791.

Gronenborn, A. M., & Clore, G. M. (1990) *Anal. Chem. 62*, 2–15.

Gronenborn, A. M., Clore, G. M., Schmeissner, U., & Wingfield, P. T. (1986) *Eur. J. Biochem. 161*, 37–43.

Howarth, O. W., & Lilley, D. J. M. (1978) *Prog. Nucl. Magn. Reson. Spectrosc. 12*, 1–40.

Ikura, M., Kay, L. E., & Bax, A. (1990a) *Biochemistry 29*, 4659–4667.

Ikura, M., Kay, L. E., Tschudin, R., & Bax, A. (1990b) *J. Magn. Reson. 86*, 204–209.

Kay, L. E., Marion, D., & Bax, A. (1989) *J. Magn. Reson. 84*, 72–84.

Kay, L. E., Ikura, M., & Bax, A. (1990a) *J. Am. Chem. Soc. 112*, 888–889.

Kay, L. E., Ikura, M., Tschudin, R., & Bax, A. (1990b) *J. Magn. Reson.* (in press).

Kay, L. E., Clore, G. M., Bax, A., & Gronenborn, A. M. (1990c) *Science 249*, 411–414.

Kraulis, P. J., Clore, G. M., Nilges, M., Jones, T. A., Pettersson, G., Knowles, J., & Gronenborn, A. M. (1989) *Biochemistry 28*, 7241–7257.

Krivdin, L. B., & Kalabin, G. A. (1989) *Prog. Nucl. Magn. Reson. Spectrosc. 21*, 293–448.

Levy, G. C., & Nelson, G. L. (1972) *^{13}C NMR for Organic Chemists*, Wiley-Interscience, New York.

Marion, D., Ikura, M., Tschudin, R., & Bax, A. (1989) *J. Magn. Reson. 85*, 393–399.

Moore, M. A. S. (1989) *Immunol. Res. 8*, 165–175.

Oppenheim, J. J., Kovacs, E. J., Matsushima, K., & Durum, S. K. (1986) *Immunol. Today 7*, 45–56.

Qian, Y. Q., Billeter, M., Otting, G., Müller, M., Gehring, W. J., & Wüthrich, K. (1989) *Cell 59*, 573–580.

Shaka, A. J., Keeler, J., Frenkiel, T., & Freeman, R. (1983) *J. Magn. Reson. 52*, 335–338.

Shaka, A. J., Barker, P. B., & Freeman, R. (1985) *J. Magn. Reson. 64*, 547–552.

Shaka, A. J., Lee, C. J., & Pines, A. (1988) *J. Magn. Reson. 77*, 274–293.

Sogn, J. A., Craig, L. C., & Gibbons, W. A. (1974) *J. Am. Chem. Soc. 96*, 4694–4695.

Torchia, D. A., Leyerla, J. R., & Quattrone, A. J. (1975) *Biochemistry 14*, 887–900.

Tran-Dinh, S., Fermandjian, S., Sala, E., Mermet-Bouvier, R., Cohen, M., & Fromageot, P. (1974) *J. Am. Chem. Soc. 96*, 1484–1493.

Wang, J., Hinck, A. P., Loh, S. N., & Markley, J. L. (1990) *Biochemistry 29*, 102–113.
Wingfield, P. T., Payton, M., Tavernier, J., Barnes, M., Shaw, A., Rose, K., Simona, M. G., Demaczuk, S., Williamson, K., & Dayer, J.-M. (1986) *Eur. J. Biochem. 160*, 491–497.
Wüthrich, K. (1986) *NMR of Proteins and Nucleic Acids*, Wiley, New York.
Wüthrich, K. (1989) *Acc. Chem. Res. 22*, 36–44.
Zuiderweg, E. R. P., McIntosh, L. P., Dahlquist, F. W., & Fesik, S. W. (1990) *J. Magn. Reson. 86*, 210–216.

Study of the Binding of Single-Stranded DNA-Binding Protein to DNA and Poly(rA) Using Electric Field Induced Birefringence and Circular Dichroism Spectroscopy†

M. E. Kuil,*,‡ K. Holmlund,§ C. A. Vlaanderen, and R. van Grondelle
Department of Physics and Astronomy, Free University de Boelelaan 1081, 1081 HV Amsterdam, The Netherlands
Received November 9, 1989; Revised Manuscript Received March 28, 1990

ABSTRACT: Binding of the single-stranded DNA-binding protein (SSB) of *Escherichia coli* to single-stranded (ss) polynucleotides produces characteristic changes in the absorbance (OD) and circular dichroism (CD) spectra of the polynucleotides. By use of these techniques, complexes of SSB protein and poly(rA) were shown to display two of the binding modes reported by Lohman and Overman [Lohman, T. M., & Overman, L. (1985) *J. Biol. Chem. 260*, 3594–3603]. The circular dichroism spectra of the "low salt" (10 mM NaCl) and "high salt" (>50 mM NaCl) binding mode are similar in shape, but not in intensity. SSB binding to poly(rA) yields a complexed CD spectrum that shares several characteristics with the spectra obtained for the binding of AdDBP, GP32, and gene V protein to poly(rA). We therefore propose that the local structure of the SSB–poly(rA) complex is comparable to the structures proposed for the complexes of these three-stranded DNA-binding proteins with DNA (and RNA) and independent of the SSB-binding mode. Electric field induced birefringence experiments were used to show that the projected base–base distance of the complex is about 0.23 nm, in agreement with electron microscopy results. Nevertheless, the local distance between the successive bases in the complex will be quite large, due to the coiling of the DNA around the SSB tetramer, thus partly explaining the observed CD changes induced upon complexation with single-stranded DNA and RNA.

The binding properties of *Escherichia coli* SSB protein, belonging to the class of single-stranded DNA-binding proteins, show many similarities with the properties of gene 32 protein and AdDBP, the single-stranded DNA-binding protein of the (eukaryotic) adenovirus [for a review, see Chase and Williams (1986)]. Only recently the rather different binding properties of the SSB protein, as compared to GP32 and AdDBP, were fully recognized by Lohman and co-workers (Lohman & Overman, 1985; Bujalowski & Lohman, 1986; Bujalowski et al., 1988). A comprehensive review covering this subject appeared recently (Lohman et al., 1988). The variety of binding modes exhibited by SSB protein depend on the salt concentration, salt type, pH, and temperature and are characterized by a different size of the binding site. Moreover, is was shown that the binding of the protein can be described more accurately assuming the "nearest neighbor cooperativity" model (McGhee & von Hippel, 1974) that successfully explained the binding properties of GP32 [see Kowalczykowski et al. (1986) and references cited therein] and recently also the binding of AdDBP to poly(rA) (Kuil et al., 1989).

The SSB protein is a multifunctional protein in the DNA metabolism of *E. coli*; it is essential for DNA replication, DNA recombination, and repair (Chase & Williams, 1986). Moreover, the protein protects the single-stranded DNA against nuclease activity. The variety of functions that the SSB protein plays in the cell may well be related to the observed different binding modes in vitro as well as to the interaction of SSB with several *E. coli* proteins [recA, pol II, exoI, and the n protein (Morrical et al., 1986; Sigal et al., 1972; Molineux & Gefter, 1975; Low et al., 1982)]. As an example, recent experiments of Kowalczykowski et al. (Kowalczykowski et al., 1987; Kowalczykowski & Krupp, 1987) have shown that the effect of the SSB protein on the ATPase activity of *E. coli* recA protein is critically dependent on the temperature, the substrate, the order of addition, and the magnesium concentration. It was shown by Kowalczykowski et al. that either the SSB protein displaces the recA protein from the single-stranded DNA or recA is able to displace the SSB protein, dependent on the presence of cofactors. In previous studies, we reported the solution dimensions of complexes of GP32 and ssDNA fragments using electric birefringence and quasi-elastic light-scattering experiments. For GP32, it was observed that the projected distance between the DNA bases increased substantially (0.53 nm compared to 0.34 nm per base for double-stranded DNA) (Scheerhagen et al., 1985a,b; Scheerhagen, 1986; Kuil et al., 1990). Moreover, it was shown that the complex has a low bending persistence length of about 35 nm (Kuil et al., 1988, 1990). An increase of the base–base distance to 0.47 nm was observed by Delius using electron microscopy for GP32 binding to fd DNA (Delius et al., 1972). For SSB, similar electron microscopy experiments were performed, indicative of a decreased base–base distance of 0.19 nm per base (using a value of 6407 nucleotides in the fd DNA)

† Supported by the Dutch Organization of Pure Research (NWO) via the Foundation of Biophysics (Stichting voor Biofysica).
‡ Present address: Department of Physical and Macromolecular Chemistry, Gorlaeus Laboratories, POB 9502, 2300 RA Leiden, The Netherlands.
§ Present address: Institute of Theoretical Physics, Chalmers University of Technology, University of Göteborg, S-41296 Göteborg, Sweden.

0006-2960/90/0429-8184$02.50/0